Optimisation of the thermal-treatment of chemically prepared electrochromic nickel oxide thin films, their electrochromic properties and structural investigations

Romana Cerc Korošec and Peter Bukovec

Faculty of Chemistry and Chemical Technology, University of Ljubljana, Aškerčeva 5, 1000 Ljubljana, Slovenia

Contents:

1. Introduction :

Non-stoichiometric nanostructured or polycrystalline nickel oxide possesses several excellent properties. It is a low cost material, which can be manufactured by a variety of physical and chemical techniques, such as the sol-gel process[1], spray pyrolysis [2], chemical vapour deposition [3], solution growth [4], chemical bath deposition [5], alternately dipping deposition [6], thermal evaporation [7], anodic electrodeposition [8], cathodic electrodeposition [9], electron beam evaporation [10], the electro-deposition method followed by thermal oxidation [11], rf reactive sputtering [12] and

DC reactive magnetron sputtering [13]. As an anodic electrochromic material it changes colour from transparent (Ni^{2+}) to deep brown (Ni^{3+}) under anodic potentials [14] and exhibits long durability and electrochemical stability in basic environments [15]. In addition it is a p-type semiconductor with a wide band gap (3.6 – 4.0 eV) [16]. In the form of a thin film it is a promising candidate for many applications such as a functional layer material for gas sensors [17], antiferromagnetic layers [18], p-type transparent conducting films [19], an ion storage layer in complementary electrochromic devices where the electrochromic layer is WO_3 [20], a dye sensitizer in solar cells [21], an optical recording material [22] and a supercapacitor [23]. Recently some full-scale electrochromic smart windows, which allow dynamic throughput control of light and solar energy and can be used as efficient solar protection against overheating, are undergoing practical testing in buildings [24]. The potential applications also include flexible-foil-type electrochromic devices for ski goggles and motorcycle helmets [20(a)]. In powdered form, nickel oxide nanoparticles can also be used as nanooxidisers for pyrotechnic purposes [25].

Nickel hydroxide and nickel oxide take part in redox processes and therefore possess electrochemical properties. The electrochromism in nickel oxide based materials probably involves several species, which differ in structure: nickel oxide (cubic NaCl structure), the hydroxide (layered structure) or oxyhydroxide (surface-hydroxylated NiO or oxidized $Ni(OH)_2$). Due to the fact that the phase transformation of nickel oxide to nickel hydroxide occurs gradually in an electrolyte solution, or that the as-prepared sample already contains more than one phase, a dichotomy in denomination among these species still exist. A lot of work in this field was done on nickel hydroxide, a material with good intercalation properties and widely used in rechargeable batteries. The basic reaction scheme for nickel hydroxide was proposed by Bode [26]. $Ni(OH)_2$ is oxidized under an anodic potential to NiOOH due to proton deintarcalation: $Ni(OH)_2 \leftrightarrows NiOOH + H^+ + e^-$. The proton then reacts with a hydroxide ion (present in the electrolyte), leading to formation of water. The topotactic reaction, occurring in the more dense structure of β-$Ni(OH)_2$, ensures excellent reversibility of the electrochemical reaction. Further investigations on the structural stabilization of $Ni(OH)_2$ were made by Faure and coworkers [27].

In order to elucidate the electrochemical mechanism which takes place during the coloration / bleaching process in nickel oxide thin films, numerous studies have been performed [28], reporting that it depends on the crystal structure of the material and on the measuring conditions [29]. In porous-structured NiO film, where a high ratio between the surface and the volume of the thin film is obtained, the following reaction has been proposed: NiO (transparent) + $OH^- \leftrightarrows$ NiOOH (brown) + e^- [13, 30]. A recent study [31] reported that in the activation period an increase in capacity occurs, corresponding to the chemical transformation $NiO + H_2O \rightarrow Ni(OH)_2$. Structural changes from NaCl type (bunsenite NiO) to layered $Ni(OH)_2$ occur upon amorphisation on the grain boundaries. In the steady state the reversible colour change from transparent to brownish involves the classical “battery” reaction: $Ni(OH)_2 + OH^- \leftrightarrows NiOOH + H_2O + e^-$. NiO grains therefore act as a reservoir of the electrochemically active hydroxide layer. Several papers have reported that reversible electrochemical oxidation of Ni-atoms located at the NiO/electrolyte interface is responsible for the strong electrochromic effect [16(c), 32], or that the electrochromic performance of nickel oxide depends on the size of the nanocrystallites [33]. Already in 1988 Estrada observed that the optical properties of a thin film, consisting of grains

about 7 nm in diameter, are stable for at least 5000 cycles, whereas for a 17 nm grain size a significant degradation was observed already after 50 cycles [34]. The decrease in electrochromic properties after prolonged cycling is associated with dissolution of the NiOOH phase structure [35]. One of the possible mechanisms responsible for the bleaching ⇆ colouring process is also the reaction at the interface between NiO and $Ni(OH)_2$: $NiO + Ni(OH)_2 \leftrightarrows Ni_2O3 + 2H^+ + 2e^-$ [20(a)].

Chemical methods of deposition are cheaper and technically less demanding than physical ones [2, 36]. The sol-gel method allows control of the variety of composition and homogeneity of the final product, as well as a lower processing temperature [37]. This method attracted increasing interest during the last few years in the preparation of thin films [38]. The thin layer can be easily deposited on the substrate by dip- or spin-coating. Unfortunately, compared to vacuum-based approaches, solution processing has not been considered as a technique that will produce high quality thin films with respect to control over the texture, growth rate, composition, and microstructure of the deposited films [39].

The starting solution in sol-gel synthesis contains the precursor salt and different additives, complexing agents or templates which enable tailoring of the desired properties of the final material. After the deposition process, an amorphous layer is formed on the substrate surface. During thermal treatment, dehydration and combustion (thermal decomposition of organic phase and constituents of the initial precursor) take place in one or more temperature regions, specific for the particular system. For the majority of the above mentioned applications the final temperature of heat treatment is chosen with the aim of achieving a semiconducting material; i.e. polycrystalline or nanosized NiO which still contains nickel vacancies, impurities or the presence of interstitial oxygen in the NiO crystallites [40]. Too high a processing temperature leads to formation of stoichiometric crystalline NiO which is an insulator. Due to its large resistivity ($> 10^{13}$ Ω cm) [41] a material of this kind does not allow proton or hydroxide ion insertion. The intercalation / extraction of one of these species is the basis of the colouration / bleaching process which takes place during application of the film [10]. The second reason could be an excessively dense structure of the material, which sterically prevents the intercalation of the mentioned species. This means that the reaction kinetics of (i) transformation of the bunsensite NiO phase at the surface of nanograins to $Ni(OH)_2$ phase and of (ii) intercalation / deintercalation (ions diffusion) is slower [42], and the material can even remain inert [43]. A highly porous structure, on the other hand, provides a large active surface area for redox reaction and as a consequence improved electrochromic properties [44].

An important parameter distinguishing between electrochromic materials is the wavelength-dependent coloration efficiency (*CE*), expressed in $cm^2\ C^{-1}$ and given by the expression [45]:

$$CE(\lambda) = \frac{\Delta OD(\lambda)}{\Delta Q} = \frac{\log(T_b / T_c)}{\Delta Q},$$

where $\Delta\, OD(\lambda)$ is the change in optical density, $T_b\,(\lambda)$ transmittance in the bleached and $T_c\,(\lambda)$ transmittance in the coloured state. ΔQ corresponds to the inserted / extracted charge as a function of unit area. A large value of *CE* means that a small amount of electric charge is required for the colour change process. Electrochromic nickel oxide thin films exhibit high coloration efficiency (*CE* between – 30 and –

50 cm^2 C^{-1}), depending on the preparation technique [45, 46]. The films prepared by various physical and chemical methods [1-13] differ in stoichiometry, structure, degree of crystallinity, crystallite size etc. As a consequence their electrochromic properties vary over a wide range. In order to improve adhesion to the substrate and to ensure structural stability during cycling in an alkaline electrolyte, electrochromic nickel-oxide thin films have to be thermally treated during or after the deposition process. A direct consequence with regard to the content of the previous paragraph is that the degree of thermal treatment is the key factor which influences the magnitude of the optical modulation and stability of the film during the cycling process, regardless of the preparation technique, Too high a processing temperature significantly lowers the electrochromic effect [28(b), 33(b), 47], and the layer can even become inactive [28(c), 33]. On the other hand, in thermally untreated films either the optical modulation decreases soon after the beginning of cycling [48], or the film becomes detached from the substrate [49]. A dependence of structural and spectroelectrochemical properties on the annealing temperature is not only well-known for nickel oxide film, but also for WO_3 thin films [2, 50], which have recently been widely used in combination with NiO in electrochromic foil-based devices.

Thermal analysis (TA) consists of a group of techniques where a change in the sample property is related to an imposed temperature alteration. Thermogravimetry (TG) is a technique in which the change in the sample mass is analysed while the sample is subjected to temperature alteration. Differential scanning calorimetry (DSC) is a technique in which the change in the heat flow rate to the sample and to a reference sample is analysed while they are subjected to a temperature alteration [51]. Both techniques, TG and DSC, provide valuable information in the field of thermal-treatment and its optimisation of different types of materials. Routine analyses are always performed on xerogel samples. Thermal analysis of thin films is a demanding procedure and direct measurements of thin films are still not very common [52]. This is the reason why in articles which report nickel oxide thin film properties the thermal analysis is either made on the corresponding xerogels [1, 28(c), 38(a), 43, 53] or the investigated films are thermally treated at 250 or 300 °C without performing TG analysis even for xerogels [16(c), 36(a)]. The thickness of thin films usually does not exceed 1 μm [52], but in some cases thermal analysis of thin films can be performed in the usual manner:

- If the thin film exists as a free-standing (self-supporting) film, for instance thin metal films (Al foil), fast quenched amorphous alloys or thin films of polymers; the sample for TA need only be cut into small pieces or powdered and placed in the crucible (summarized examples are collected in [54]),
- If the thin film is deposited on a powdered substrate (TiO_2 on mica); a large active area of the substrate ensures enough sample for classical analysis [55],
- If the thickness of the thin film exceeds 1 μm; the thin film can be mechanically removed from the substrate [56].

When the film is very thin (< 100 nm), it is difficult to get enough sample for analysis by scraping, but there are some methods for separating a thin film from the substrate [57]. However, it should be emphasized that when the sample is prepared as a thin film or in powdered form, the differences in the particle size and in microstructure of the two forms lead to different thermal stabilities. It is well known that the decomposition temperature decreases with decrease in sample particle size [58] and

that the results obtained for deposited thin film samples and the corresponding xerogels can differ considerably due to differences in sample size, structure and microstructure [54, 59]. Thermal decomposition of sol-gel derived thin films occurs at lower temperatures than that of xerogels [60]. Explanation of the stoichiometric or structural properties of a thin film obtained from the results from TG and DSC curves of xerogels can lead to a wrong interpretation.

The sensitivity of balances in TG instruments is in the order of 1 μg so that detection of the thermal decomposition of thin films deposited on a substrate is possible [61]. But the amount of sample available is small, typically below 1 mg, so that the mass change during TG experiment is in the range of buoyancy and aerodynamic effects. In DSC measurements the evolved or absorbed heat diffuses into the substrate and consequently the measured enthalpies are very small [62]. In order to overcome these problems, large area samples have been used [63] or measurements carefully performed - for instance subtraction of the blank curve [62], high resolution TG [64] or the thin film was placed directly on the sample thermocouple in DSC measurements [65]. The mentioned basic strategies for overcoming the above-mentioned difficulties were published in the 1990-ies in three review papers [54, 61, 62]. The suggestions are summarized in Figure 1.

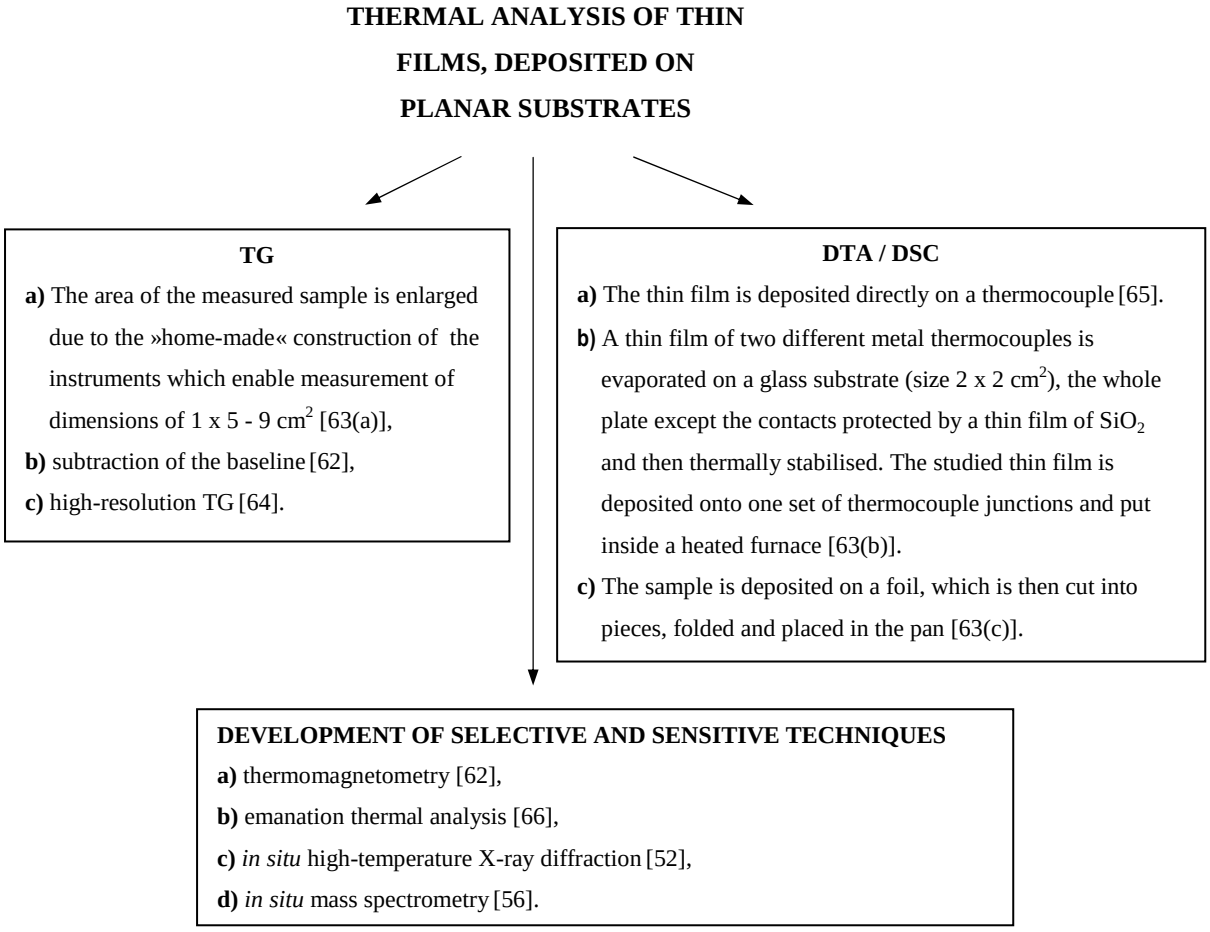

Figure (1) **:** Basic strategies applied in thermal analysis of thin films, deposited on planar substrates.

1.2 Scope of the work :

The main idea was to link the thermal analysis of thin films with the temperature-dependent electrochromic response of nickel oxide films. The first aim was a comparison between dynamic and isothermal TG curves of thin films and xerogels, prepared by the sol-gel route from $NiSO_4$ and $Ni(CH_3COO)_2$ precursors. Another preparation route was alternately dipping deposition, where $NiSO_4$ was again used as the precursor. On the basis of isothermal TG analysis, films with different ratios between the thermally undecomposed amorphous phase and nanosized Ni oxide were prepared. Their electrochromic properties were tested with additional spectroelectrochemical measurements, while changes in their structure and morphology during thermal decomposition were followed using Fourier transform infrared spectroscopy (FT-IR), transmission electron microscopy (TEM), atomic force microscopy (AFM) and Extended X-ray Absorption Fine Structure (EXAFS) analysis. As far as we know, this approach for optimising the electrochromic response has never been used before.

Thin film samples with a thickness of less than 50 nm were used to perform all of the measurements (also FT-IR spectroscopy in the transmission mode and EXAFS).

2. Results and Discussion

2.1 Thin films prepared by the sol-gel method from nickel sulfate precursor

2.1.1 Preparation of the sol and xerogel; thin film deposition :

2.0 M LiOH solution (Kemika, Zagreb, Croatia) was added dropwise with stirring to a 0.5 M solution of nickel sulfate (Kemika) until pH 9.0 was reached. The green precipitate was washed several times with water. The slurry was then peptised with glacial acetic acid to pH 4.5. Some water was added to obtain an appropriate viscosity. The sol was then sonicated and filtered. To obtain the corresponding xerogel, the sol was cast in a Petri dish and left to dry.

Thin films were prepared on different substrates using the dip-coating technique. For TG measurements the substrates used were microscope-cover glasses. For DSC measurements a small home made platinum disc with a diameter 6 mm was used. For IR measurements, the films were deposited on Si wafers and for spectroelectrochemical measurements on SnO_2/F glass (square resistivity 13 Ω/□). Before deposition, a wetting agent was dispersed on all types of substrates, using the dip-coating technique. For glasses and Si resins a solution of 1 wt. % of Etolat TD-60 (TEOL Factory, Ljubljana, Slovenia) in distilled water was prepared, while for the platinum disc and SnO_2/F glass a solution of 1 wt. % of Teloxide (TEOL Factory, Ljubljana, Slovenia) in ethanol was used. After the wetting solution had dried, the thin film was deposited with a pulling velocity of 5 cm min^{-1}. The Instrumentation is given in detail in Refs. [1(b,d)].

2.1.2 Thermal analysis :

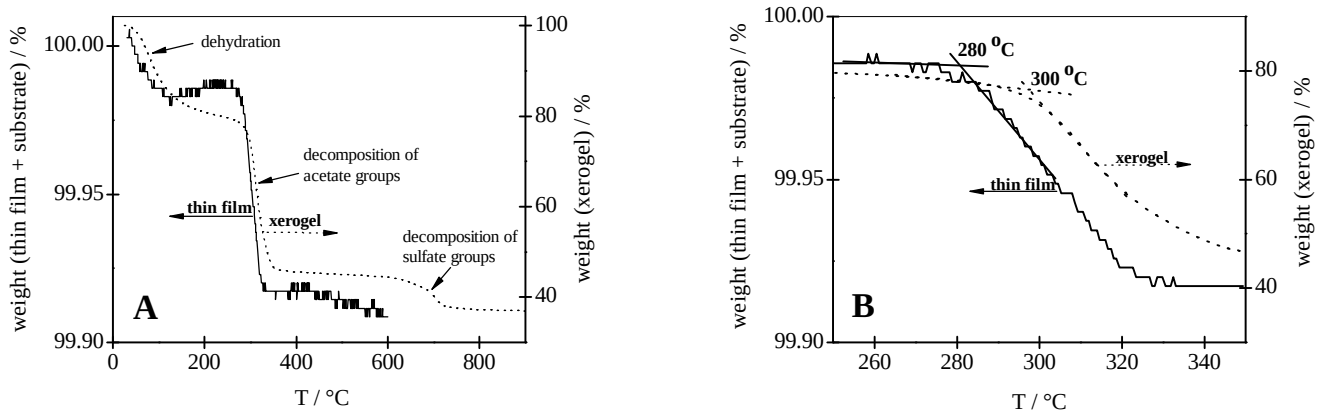

Figure (2) : Comparison of dynamic TG curves of a thin film deposited on a microscope cover glass (left ordinate), and of the xerogel (right ordinate), in a dynamic air atmosphere – A, and magnification of the temperature region where thermal decomposition of acetate groups takes place – B.

Dynamic thermogravimetric measurements of a thin film and the corresponding xerogel powder under an air atmosphere are presented in Figure 2. The calculated substrate to film mass ratio was 580 and the initial mass of the film deposited per square centimetre of substrate was 0.064 mg cm^{-2} [1(b)]. Due to the low sample mass and large dilution effect, two phenomena can be observed in the dynamic TG curve of the thin film. Firstly, the curve is not smooth because the very small mass loss (~ 0.1 % in the whole temperature range), means that the digital noise of the instrument was appreciable. Secondly, in the temperature range from approx. 100 to 200 °C a slight increase in weight was observed. Although the baseline (TG curve of empty pan) was subtracted, small variations in the flow rate of the purging gas may have caused a weight gain.

From room temperature up to 200 °C only water molecules were evolved from the sample [1(b)]. The second step on the TG curves occurred due to thermal decomposition of acetate groups. Combustion of these groups was also proved with the coupled TG-MS technique. Combining TG measurements with gas-analytical techniques significantly enhances the possibilities for correctly interpreting the mechanisms of thermally induced reactions which involve gaseous species [67]. During thermal decomposition of acetates (see the evolution of the IR spectra in Fig. 7) nano-grains of nickel oxide were formed inside the sample (TEM micrograph, Fig. 9B). The onset decomposition temperature of acetate groups was 280 °C for the thin film sample and 300 °C for the xerogel (Fig. 2B). The third step in the TG curve of the xerogel around 700 °C was attributed to thermal decomposition of the sulfate groups which remained coordinated to nickel cations during the preparation of the sol [1(b)]. The dynamic TG measurement was performed only to 600 °C for the thin film sample; above this temperature microscope cover glasses began to soften.

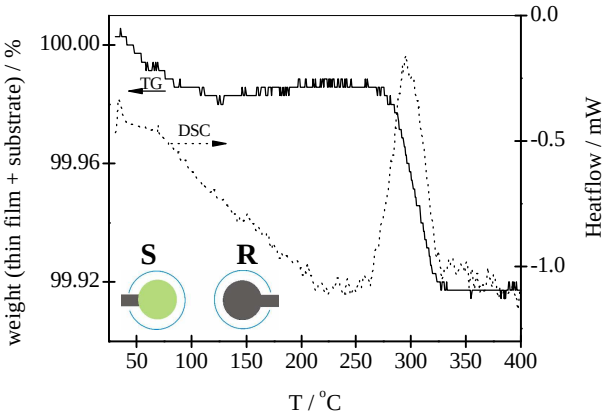

Figure (3) : Dynamic TG curve of a thin film deposited on a glass substrate (left ordinate) and the DSC curve of a thin film placed directly on the thermocouple (right ordinate). An undeposited Pt disc served as a reference.

The DSC curve of the film deposited on a platinum disc and placed directly on the thermocouple is shown in Figure 3 together with the dynamic TG curve. The exothermic signal on the DSC curve coincided with the weight loss in the temperature range where acetate groups thermally decompose. In the case of a thin film deposited on an aluminium foil, cut into small pieces, placed in an Al pan and covered with a pierced lid ("classical" DSC measurement), higher onset and endset temperatures were determined because the equilibrium reaction was restored between the thermally undecomposed solid phase and the gas phase formed during decomposition [1(b)].

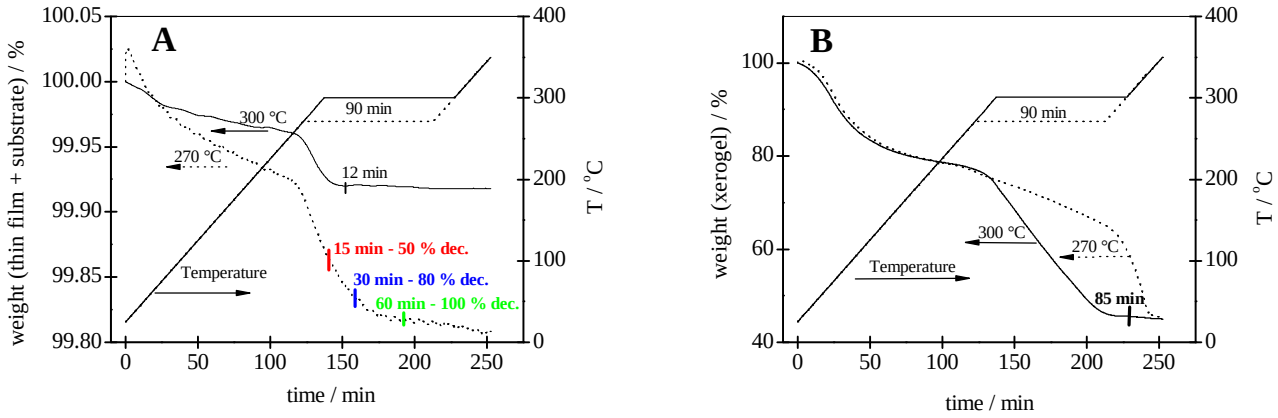

Figure (4) : Isothermal TG curves of a thin film – A, and of the corresponding xerogel – B at 270 °C and at 300 °C.

Isothermal TG curves of both forms of sample at 270 and 300 °C are shown in Figures 4A, B. The temperature was chosen on the basis of dynamic measurements of the thin film and the xerogel (Fig. 2B). After isothermal treatment the temperature in the furnace was increased to 350 °C where decomposition was complete for both

types of samples. From the ratio of the isothermal weight loss after a defined time and the weight loss associated with decomposition of all acetate groups, the degree of thermal decomposition of acetates could be estimated. For the thin film the degree of thermal decomposition was 50 % after 15 min, 80 % after 30 min and 100 % after 60 min (Fig. 4A). Only 30 % decomposition of the xerogel was observed at 270 °C after 60 min (Fig. 4B). From analogous measurements at 300 °C we noted that the thermal decomposition of the xerogel was complete after 85 min, while for the thin film is was complete after 12 min. Thin films with different ratios between the thermally undecomposed amorphous phase and nickel oxide could be prepared by controlling the time of heat-treatment at 270 °C. At 300 °C the decomposition process was much faster and the stoichiometry of the decomposition could not be exactly controlled.

2.1.3 *In-situ* spectroelectrochemical measurements :

Cyclovoltammetric (CV) measurements and *in-situ* monochromatic spectral transmittance changes (λ = 480 nm) of thin films, thermally treated to varying extents, are shown in Figures 5A, B (1st cycle) and C, D (100th cycle). During the anodic scan the oxidation of Ni^{2+} to Ni^{3+} causes coloration of the film and consequently the transmittance decreased. In the reverse scan the reduction of Ni^{3+} lead to bleaching of the film. The maximal change in transmittance between the coloured and the bleached state in the 1st cycle was exhibited by a film heat treated for 15 min at 270 °C (43.1 %). However, the decrease in the transmittance of the film in its bleached state by 1.9 % at the end of the cycle showed that the reduction was not totally reversible. Films heat treated for 30 or 60 min at the same temperature (270 ^{o}C) possessed better reversibility (Fig. 5B). CV measurements of these films (Fig. 5A) were in accordance with the observed optical properties. The higher current densities indicated a greater number of active nickel ions for the least heat treated film (15 min at 270 ^{o}C), and the positions of the anodic and cathodic peaks revealed a more compact structure in those films exposed for 30 or 60 min to 270 °C. During the cycling process the number of active nickel ions increased: in the 100th cycle current densities were approximately 2.5 times higher than in the 1st cycle (Figs. 5A, C). Approximately 50 cycles needed to be performed to complete the activation period and reach the steady state. A film which was exposed for 60 min to 270 °C, exhibited excellent reversibility in the 100th cycle. The transmittance change of 46.5 % was smaller than for a thin film kept for 30 min at the same temperature (51.5 %), but the latter did not bleach to the initial value in the 100th cycle (Fig. 5D). The calculated *CE* for a film exposed at 270 ^{o}C for 60 min was – 41 $cm^2\ C^{-1}$(λ = 480 nm) in the 100th cycle.

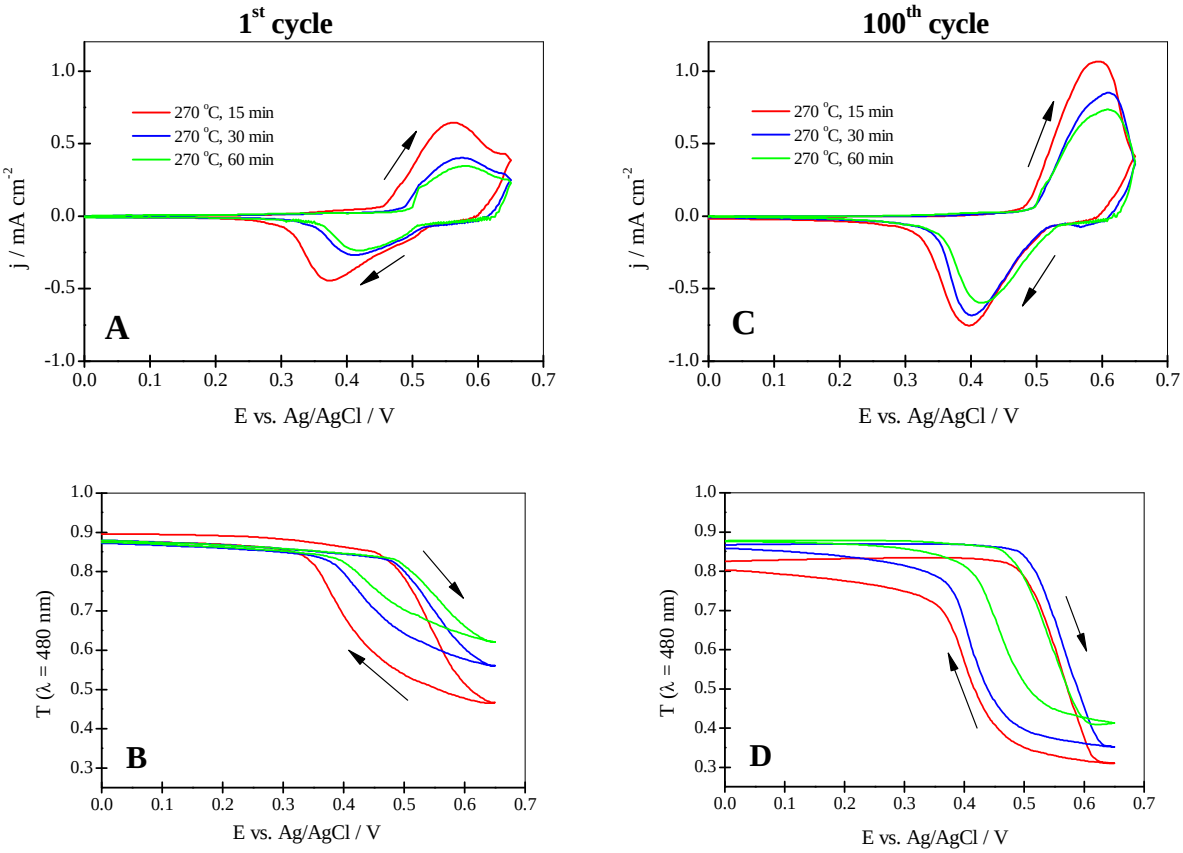

Figure (5) : Cyclovoltammetric curves and *in-situ* monochromatic transmittance changes of different thermally treated Ni oxide films in 0.1 M LiOH – 1st cycle (A, B) and 100th cycle (C, D).

Figure 6 presents the *in-situ* monochromatic transmittance change ($\lambda = 480$ nm) during chronocoulometric measurements of thin films thermally treated to different extents. The responses of the stabilized 101st cycle during charging at a potential of 0.6 V vs. Ag/AgCl (0 – 30 s) and discharging (30 – 60 s) are shown. For less thermally treated films it took around 10 s to obtain a finally coloured state (a, b), while for more thermally treated films the time increased to around 15 s (c). For a thin film treated for 15 min at 500 °C (d), approximately 13 s was needed.

Of all films the highest coloration effect was exhibited by a thin film exposed for 60 min to 270 °C. Reversibility in the bleaching process was also achieved for films thermally treated for 15 min at 500 °C (transmittance change in the 100th cycle 34.5 %), but during further heating (> 300 °C) the nano grains increased in size. The average size of the grains was 5 nm in a film treated for 15 min at 500 °C (Fig. 9C). In this film, sulfate ions remained monodentately bonded to nickel (Fig. 7, e). Assuming that electrochemical reaction takes place on the surface of the nano-grains, the coloration effect was less pronounced in films which consisted of larger grains and had smaller specific surface values. Segregation of the grains could not be observed by TG measurements, since this process is not associated with a weight loss. There

was also no measurable change in heat flow signal on the DSC curve of a thin film between 300 and 400 ^{o}C (Fig. 3).

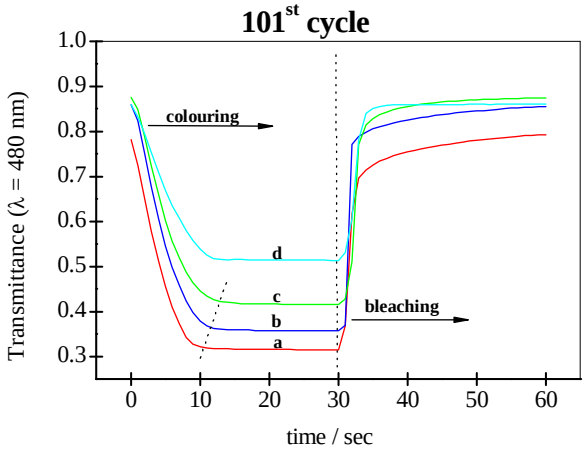

Figure (6) : *In-situ* monochromatic transmittance changes (λ = 480 nm) during chronocoulometric measurements of a thin film thermally treated at 270 ^{o}C for 15 min (a), at 270 ^{o}C for 30 min (b), at 270 ^{o}C for 60 min (c), at 500 ^{o}C for 15 min (d). The films were coloured at 0.6 V for 30 s and bleached at 0.0 V for 30 s.

2.1.4 Structural and morphological properties :

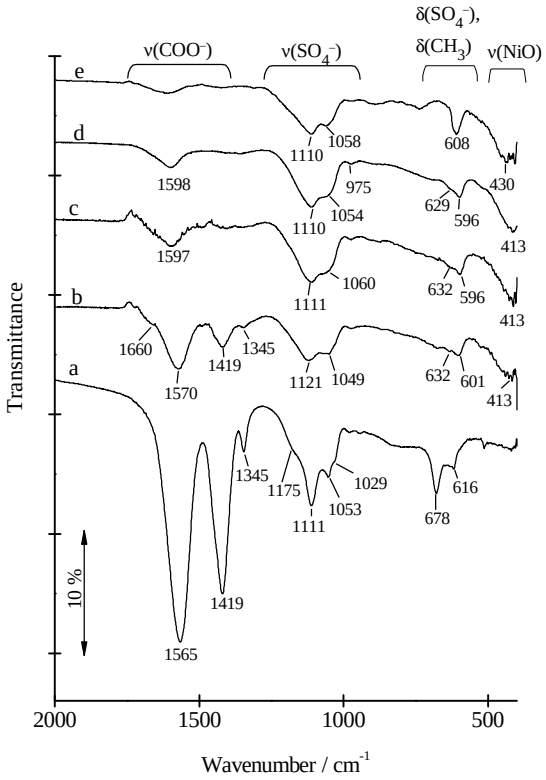

Figure (7) : IR transmittance spectra of films deposited on silicon wafers: thermally untreated film (a), film thermally treated for 15 min at 270 ^{o}C (b), for 30 min at 270 ^{o}C (c), for 60 min at 270 ^{o}C (d) and for 15 min at 500 ^{o}C (e).

The evolution of IR spectra during heat treatment is shown in Figure 5. In the IR spectrum of a thermally untreated film (Fig. 5, a) the bands at 1565 and 1419 cm^{-1} belong to asymmetric ($\nu_a(COO^-)$) and symmetric ($\nu_s(COO^-)$) vibrations of the acetate groups [28]. $\nu_a(COO^-)$ and $\nu_s(COO^-)$ for free acetate ions are at 1556 and 1413 cm^{-1}, their difference being 144 cm^{-1}. On the basis of this difference ($\Delta\nu$) one can deduce the type of coordination of the acetate groups to the metal ions [68]. Regarding the free ion, $\Delta\nu$ in the bridging complex remained practically unchanged. We can therefore suppose that in the thermally untreated film the acetate groups were mostly present as bridging ligands to nickel ions. The peaks at 1345, 1053 and 1029 cm^{-1} revealed the presence of methyl groups ($\delta(CH_3)$). The band at 1111 cm^{-1} belonged to a stretching vibration of the free sulfate groups with T_d symmetry, and the shoulder around 1175 cm^{-1} to the bridging sulfate groups with $C_{2\nu}$ symmetry [68]. Comparison of the two intensities showed that some SO_4^{2-} groups were also adsorbed on colloidal particles. The bending vibration of the free sulfate anion is at 613 cm^{-1} and that of a bridging one at 641, 610 and 571 cm^{-1}. All peaks except that at 571 cm^{-1} were of strong intensities. In the thermally untreated sample the out-of-plane vibration of acetate groups was superimposed on the bending vibration of the sulfate groups, and therefore the latter were not clearly expressed. The band at 678 cm^{-1} was attributed to the δ(OCO) vibration and that at 616 cm^{-1} to π(COO), π(CH), as well as to SO_4^{2-} bending vibrations.

The bands associated with the acetate motions became smaller in the IR spectrum of the thin film thermally treated at 270 °C for 15 minutes (Fig. 7, b). The vibrations at 1121 and 1049 cm^{-1} were attributed to stretching vibrations of the monodentately coordinated sulfate groups and those at 632 and 601 cm^{-1} to the bending vibrations of the same groups. The band that appeared below 500 cm^{-1} corresponded to a stretching vibration of the Ni-O bond of nickel oxide [27(a)]. The shoulder around 1660 cm^{-1} could be ascribed to the C=O groups bonded on organic ($-CH_2$, $-CH_3$) groups and monodentately coordinated to nickel [68]. The appearance of the carbonyl vibration revealed the reorganization of atoms and bonds during thermal decomposition of the acetate groups.

With increasing time of heat treatment at 270 °C the vibrations of the sulfate groups as well as the Ni-O stretching band became more intense (Fig. 7, c, d). The sulfate groups remained monodentately bonded to nickel (ν_3 = ~1110, 1060 cm^{-1}, ν_1 = 970 cm^{-1}, ν_4 = ~ 630 and 595 cm^{-1}). The band at ~1600 cm^{-1} was attributed to the bending vibration of water arising from absorbed moisture. A thin film thermally treated at 270 °C for 60 min consisted of nano-crystals of cubic NiO with a size of 2-3 nm, as shown in the TEM micrograph (Fig. 9B). The IR spectrum of a film thermally treated at 500 °C for 15 min revealed no appreciable difference with regard to the previously described spectrum (Fig. 7, e). From the TEM micrograph (Fig. 9C) it is clear that the grains of cubic NiO have grown to around 5 nm.

Changes of the surface during heat treatment are shown in Figure 8. The surfaces of the thin film samples (Figs. 8B, C and D) were not smooth. The reason lay in the roughness of the substrate itself (Fig. 8A), where the RMS roughness was 35 nm. After deposition of the sol, a nearly smooth surface was obtained (8B). During heat treatment the film became thinner due to thermal decomposition and the surface more

and more resembled that of the substrate (8C, D). The RMS roughness was 10 nm in sample C and 18 nm in sample D.

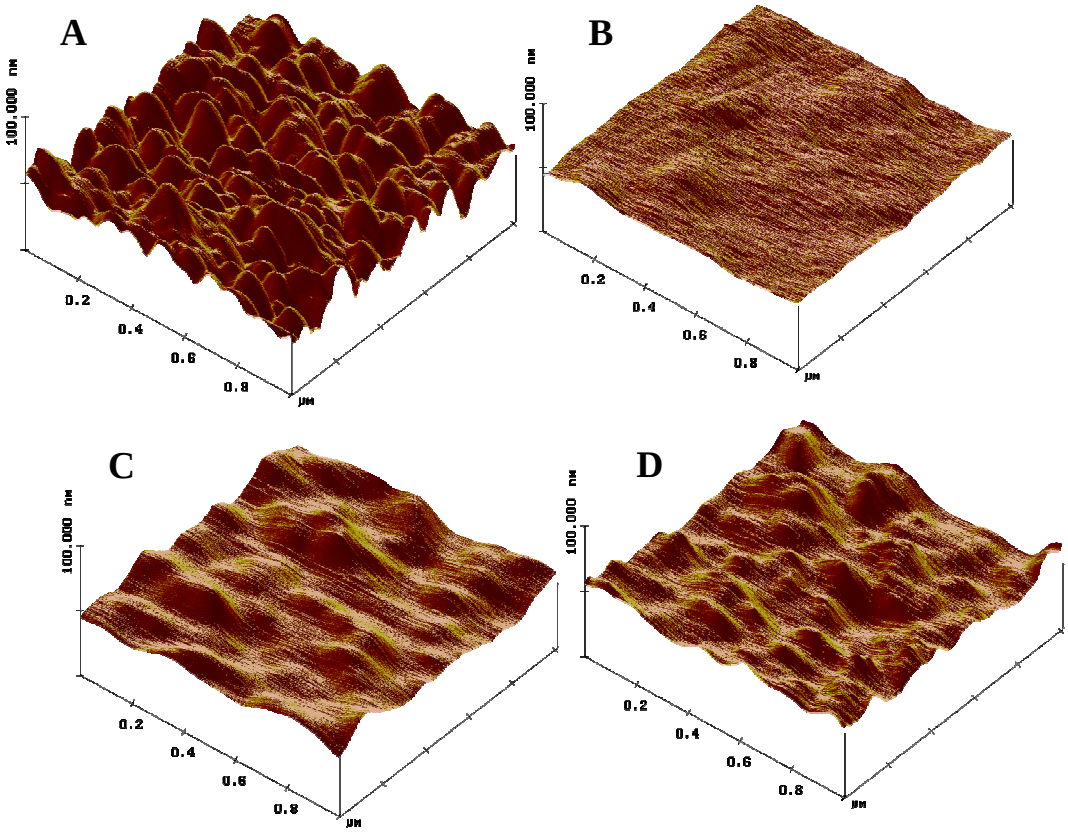

Figure (8) **:** AFM images of a SnO_2/F surface – A; surface of a thermally untreated film after the dip-coating process – B; after thermal treatment at 270 ^{o}C for 15 min – C; and after thermal treatment at 270 ^{o}C for 60 min – D.

TEM micrographs of an optimised film deposited on silicon resin (Figure 9) show a uniform layer with a thickness of 35 nm (A), consisting of nano-crystals of cubic NiO of size from 2 to 3 nm (B).

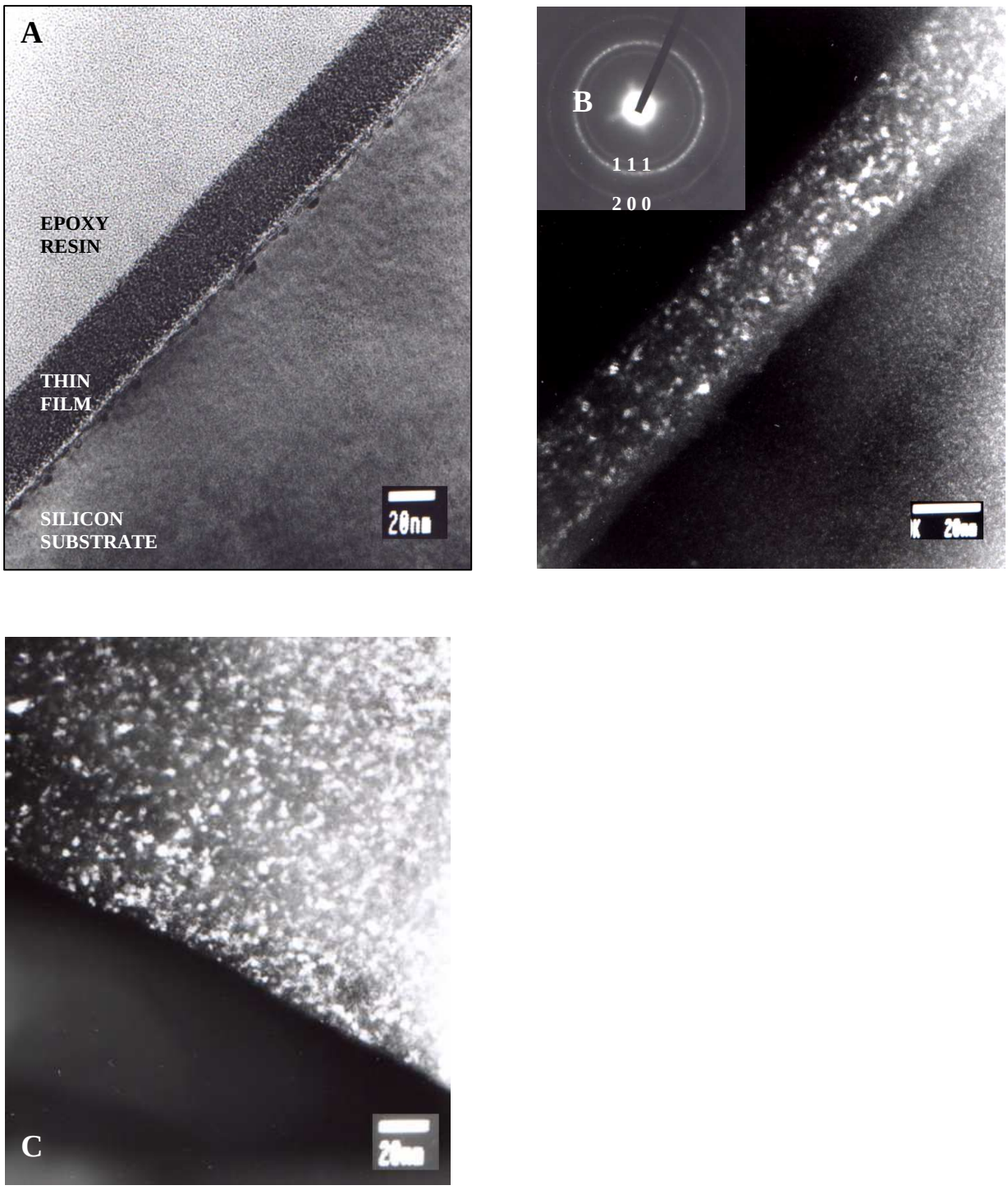

Figure (9) **:** TEM micrograph of a thin film thermally treated at 270 ^{o}C for 60 min (cross section – A), dark field image and Selected Area Electron Diffraction (SAED) pattern (inset, indexed as cubic NiO – B) of the same film, and in plan-view of a thin film, thermally treated at 500 ^{o}C for 15 min – C.

The results obtained by Auger electron spectroscopy additionally confirmed and completed the results. In Figure 10 the depth profile of a film deposited on a SnO_2/F substrate and thermally treated at 270 ^oC for 30 minutes is presented. Tin was already present just below the surface due to the morphology of the substrate itself (Fig. 8A). Its concentration increased along the profile, while the concentration of nickel decreased. At a thickness of 35 nm the concentration of tin and oxygen became constant, while that of nickel reached zero, which was in accordance with the TEM cross section (Fig. 9A). The thermal decomposition of acetates was 80 % in this film (Fig. 4A) and therefore carbon was still present in the sample. A small amount of sulphur was also detected due to presence of sulphate ions in the structure.

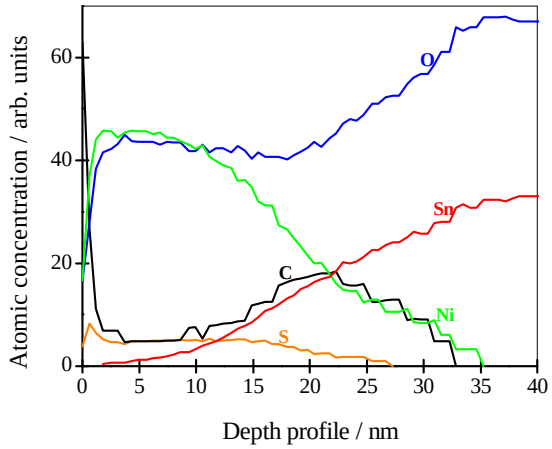

Figure (10) : In-depth composition of a thin film deposited on a SnO_2/F substrate and thermally treated at 270 ^oC for 30 min.

2.2 Thin films prepared by the sol-gel method from nickel acetate precursor

2.2.1 Preparation of the sol and xerogel; thin film deposition :

2.0 M LiOH (Kemika, Zagreb, Croatia) was added dropwise with stirring to a 0.5 M solution of nickel acetate (Kemika) until pH 9.0 was reached. The green precipitate was separated from the mother liquor by centrifugation. Then the slurry was peptised with glacial acetic acid until pH 4.5 was reached. Some water was added to obtain an appropriate viscosity. The sol was then sonicated and filtered. An analogous procedure as described above for the films prepared from $NiSO_4$ precursor was used to prepare thin films on substrates and the corresponding xerogel.

2.2.2 Thermogravimetric measurements :

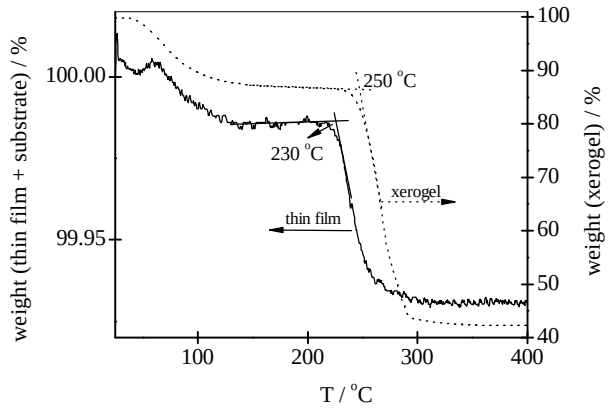

Figure (11) : Comparison of a dynamic TG curve of a thin film deposited on a microscope cover glass (left ordinate) and the corresponding xerogel (right ordinate).

Dynamic TG curves of of a thin film and the xerogel are presented in Figure 11. From room temperature up to 150 °C dehydration took place. At temperatures higher than 200 °C thermal decomposition of acetate groups occurred. The value of the onset decomposition temperature for the thin film was 230 °C and for the amorphous xerogel 250 °C. In the temperature range from 200 to 300 °C the xerogel lost 44.4 % of its weight. Assuming that the same chemical process occurs during thermal decomposition of the thin film and the xerogel, the initial mass of the thin film (without substrate) could be calculated. From this information the substrate to film mass ratio was determined, and found to be approximately 800 [1(c)].

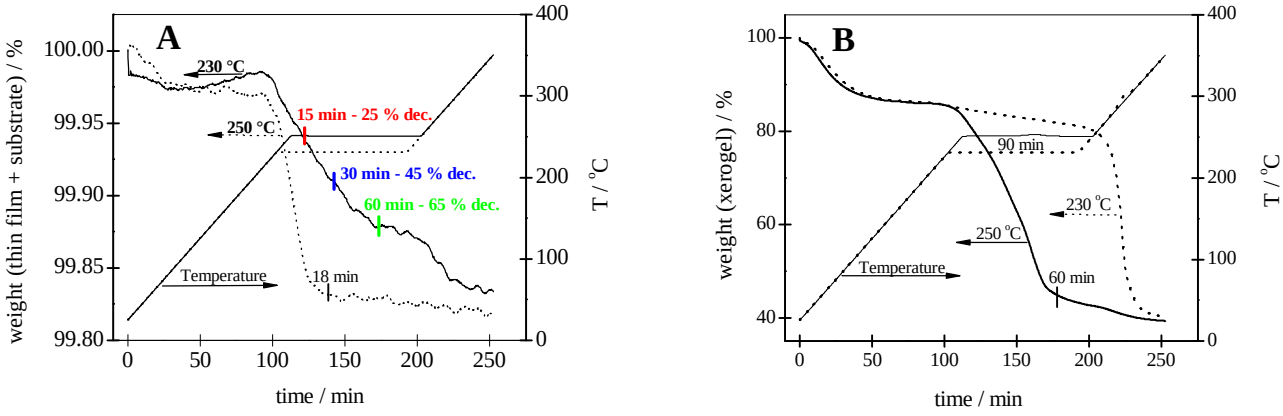

Figure (12) : Isothermal TG curves of a thin film – A, and the corresponding xerogel – B at 230 and 250 °C.

Isothermal TG curves measured at 230 and at 250 °C for the thin film and the xerogel prepared from $Ni(CH_3COO)_2$ precursor, are shown in Figures 12A, B. The isothermal temperatures were chosen on the basis of dynamic measurements (Fig. 11). The thermal decomposition of acetate groups at 230 °C in the thin film sample was 25 % after 15 min, 45 % after 30 min and 65 % after one hour (Fig. 12A). At 250 °C

decomposition was complete after approximately 20 min. In the xerogel sample only 8 % decomposition was observed after one hour at 230 °C (Fig. 12B). At 250 °C the decomposition of acetate groups was 90 % after 60 min. On the basis of the isothermal TG curve of the thin film at 230 °C, several thin films could be prepared with different ratios between the nanosized nickel oxide phase, which was formed during the decomposition process, and the thermally undecomposed amorphous phase.

2.2.3 *In-situ* spectroelectrochemical measurements :

In-situ spectroelectrochemical measurements of thin films thermally treated to varying extents are shown in Figure 13. CV measurements of the 1^{st} and 100^{th} cycles are represented in Figs. 13A, C, while *in-situ* monochromatic spectral transmittance changes (λ = 480 nm) of the corresponding cycles are shown in Figs. 13B,D. In the thermally untreated film oxidation of Ni^{2+} ions caused a large change in transmittance, i.e. from 0.90 at the beginning of the cycle to 0.43 at the end of the anodic scan, but the reduction process did not bleach the layer to the initial value (Fig. 13B). A decrease in the transmittance value of the film in its bleached state of 4.1 % was observed. Both thermally treated films exhibited very little colour change during the oxidation process in the first cycle. The current density of the thermally untreated film was large compared with the other two films (Fig. 13A). In the film which was exposed for 60 min at 230 ^{o}C, no anodic and cathodic peaks were revealed in the 1^{st} cycle. Up to the 100^{th} cycle the anodic current density of the thermally untreated film diminished and the cathodic current density became a little larger, but the transmittance was only 0.74 in the bleached state. For both thermally treated films current densities became approximately 3 times larger, and the observed transmittance change during the oxidation / reduction process was approximately 40 %. The initial transmittance value for the film thermally treated at 230 °C for 60 min was even 6 % larger than at the beginning of cycling. Reversibility of the bleaching process for these films was achieved before the thermal decomposition of acetate groups was completed. The best electrochromic properties up to 100^{th} cycle were exhibited by a film thermally treated at 230 °C for 15 min (this means only 25 % decomposition of acetate groups) At least 75 % of the film was still amorphous, but the size of the NiO grains already reached around 5 nm (Fig. 16B). The monochromatic transmittance change was 40.6 % in the 100^{th} cycle and the calculated coloration efficiency *CE* – 38 cm^2 C^{-1}. Films with a higher degree of heat treatment possessed poorer electrochromic behaviour. The monochromatic transmittance change of a film exposed for 30 min at 230 ^{o}C was 28.8 % in the 100^{th} cycle, and 34.9 % for a film exposed for 60 min at 230 ^{o}C (λ = 480 nm). The latter result was surprising, and comparison of Figs. B and D showed that the initial transmittance of this film was higher after prolonged cycling. Some Ni^{3+} ions were probably present in the as prepared heat-treated film, which after the activation period were transformed to Ni^{2+} at the initial potential. The electrochromic performance of a film treated for 15 min at 300 ^{o}C was poor (result not shown here). Its monochromatic transmittance change was 18.6 % in the 100^{th} cycle. The size of some of the NiO grains in this film reached around 8 nm (Fig. 16D).

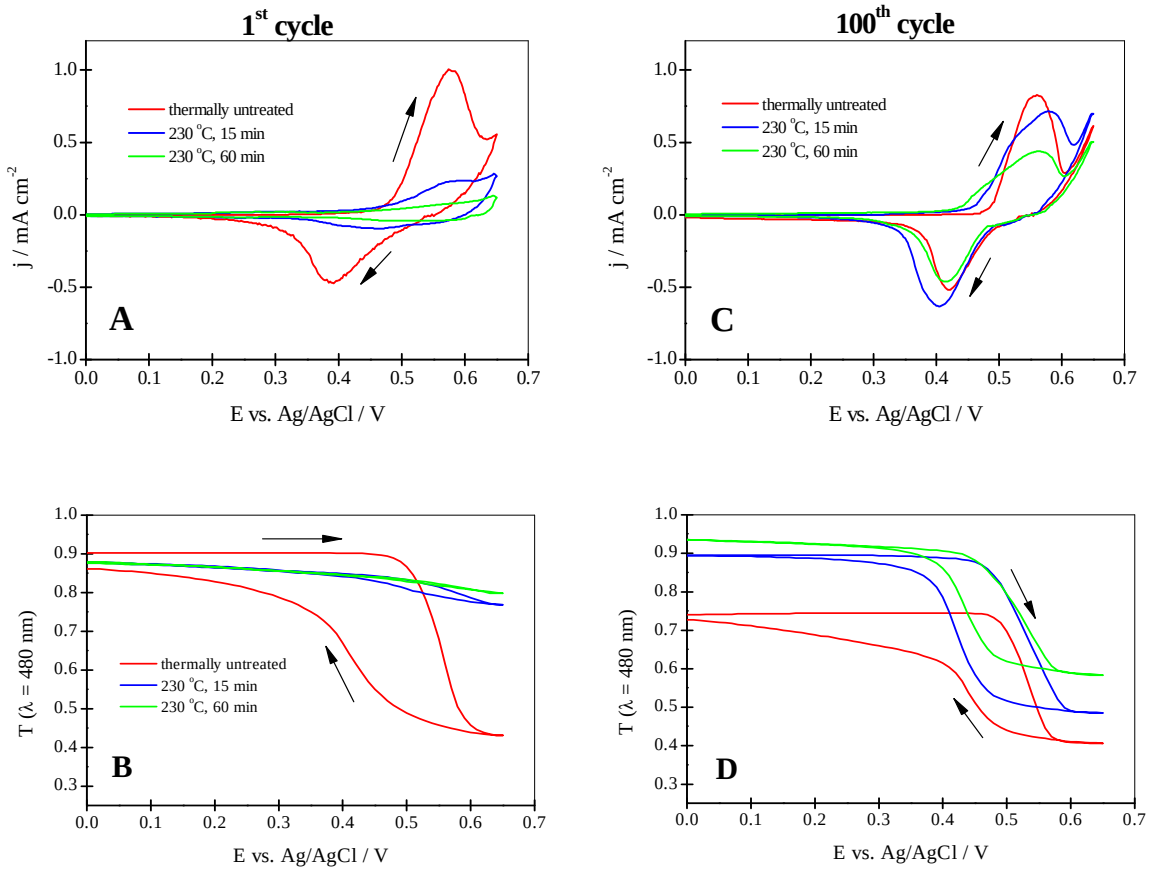

Figure (13) : Cyclovoltammetric curves and *in-situ* monochromatic transmittance changes of differently thermally treated Ni oxide films in 0.1 M LiOH – 1st cycle (A, B) and 100th cycle (C, D).

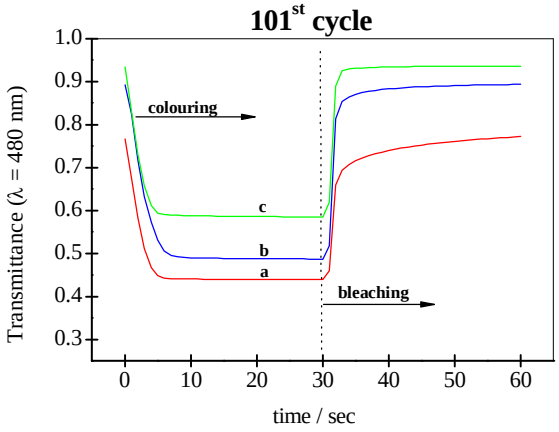

Figure (14) : *In-situ* monochromatic transmittance changes (λ = 480 nm) during chronocoulometric measurements of a thermally untreated film (a), at 230 °C for 15 min (b), at 230 °C for 60 min (c). The films were coloured at 0.6 V for 30 s and bleached at 0.0 V for 30 s.

The rate of the coloration / bleaching process of the stabilized 101st cycle is evident from Figure 14, where *in*-situ monochromatic transmittance changes (λ = 480 nm) during chronocoulometric measurements are shown. About 8 s was needed for the thermally untreated film (change in transmittance during coloration was 32.7 %) and the film exposed for 15 min to 230 ^{o}C (change in transmittance 40.6 %) to achieve their full colour, whereas for more thermally treated film (change in transmittance 34.9 %) only around 5 s was required. After switching the potential to 0.0 V vs. Ag/AgCl, the bleaching process took place and a quick increase in transmittance was observed for all films. Films which were sufficiently thermally treated to exhibit a reversible change in transmittance reached the starting value of transmittance after 5 s. On the contrary, in films where the bleaching was not reversible, after 5 s a gradual and slow increase was observed, approaching the starting value. The same behaviour is observed in Figs. 13B, D.

2.2.4 Structural and morphological properties :

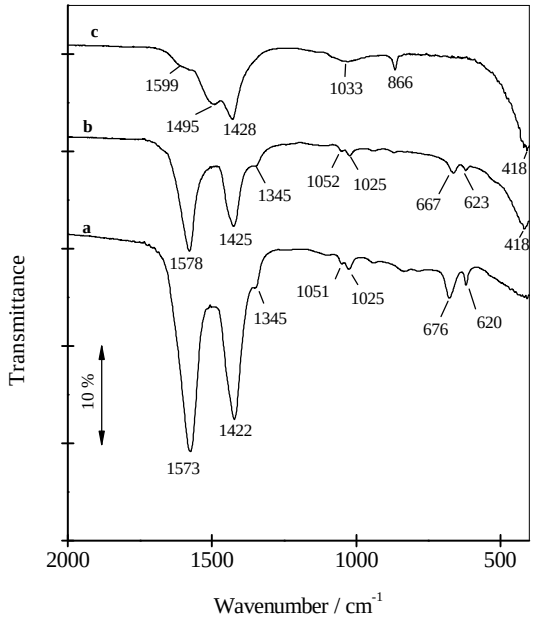

Figure (15) : IR transmittance spectra of the as deposited thin film (a), film thermally treated at 230 °C for 15 min (b) and at 230 °C for 60 min (c).The thin films were deposited on a Si wafer.

Evolution of the IR spectra of the films, thermally treated to various extent, are shown in Figure 15. In the thermally untreated film (Fig. 15, a) the bands at 1573 and 1422 cm^{-1} belong to asymmetric ($\nu_a(COO^-)$) and symmetric ($\nu_s(COO^-)$) vibrations of the acetate group [68]. The vibrations of the methyl group are revealed at 1345, 1051 and 1025 cm^{-1}. The band at 676 cm^{-1} arises from the bending vibration of the acetate group (δ(OCO)), and that at 620 cm^{-1} is attributed to the π(COO) or π(CH) vibration. When the thin film was exposed at 230 °C for 15 min the intensity of vibrations due to the presence of the acetate group decreased (Fig. 15, b). The new band appearing at 418 cm^{-1} corresponded to the stretching vibration of NiO [27(a)]. Vibrations of carbonate groups appear in the IR spectrum of the film which was heated for 60 min

at 230 °C (Fig. 15, c). The bands at 1599 and 1033 cm^{-1} correspond to the stretching ($C\text{-}O_{II}$) and to ($C\text{-}O_{I}$) vibrations of a bidentately coordinated carbonate ion [68], whereas the vibrations at 1495, 1428 and 866 cm^{-1} belong to vibrations of a free carbonate ion (D_{3h} symmetry) [68]. The results of IR spectroscopy show that during thermal decomposition a proportion of the carbonate ions, which originated from acetate groups, remained either adsorbed on the grains of nanosized nickel oxide or bound to the nickel cation via two oxygen atoms.

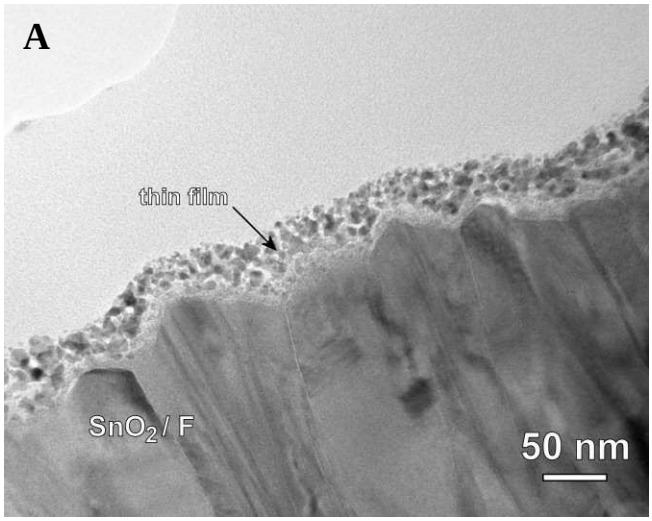

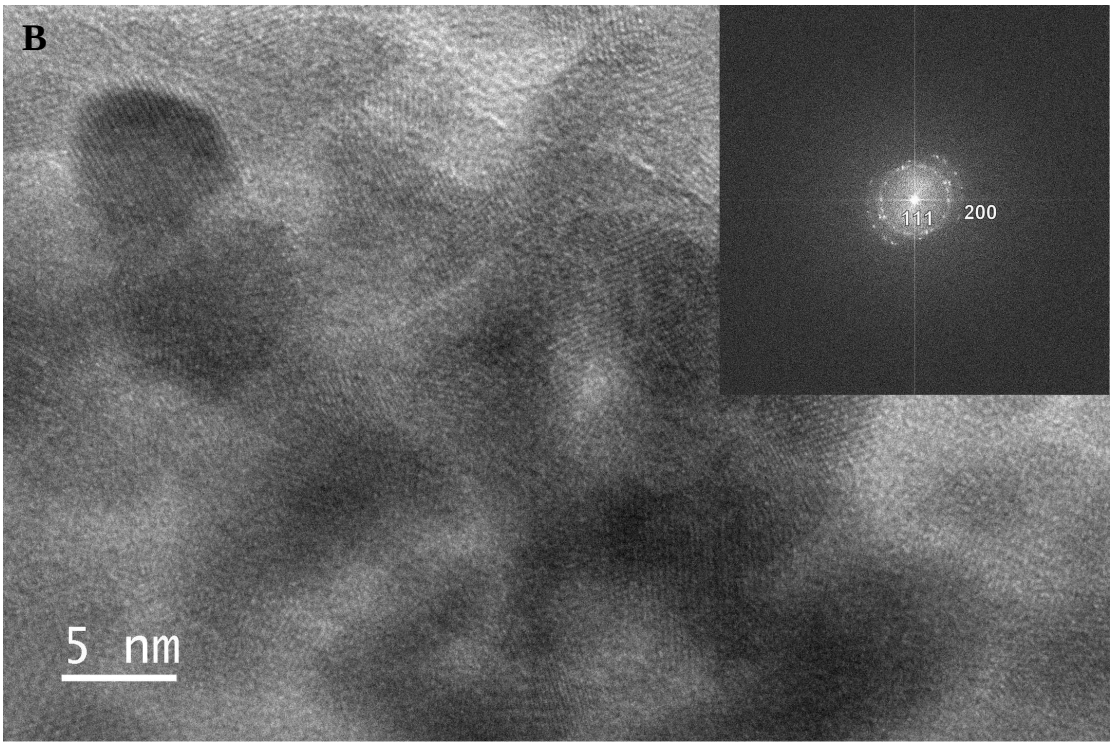

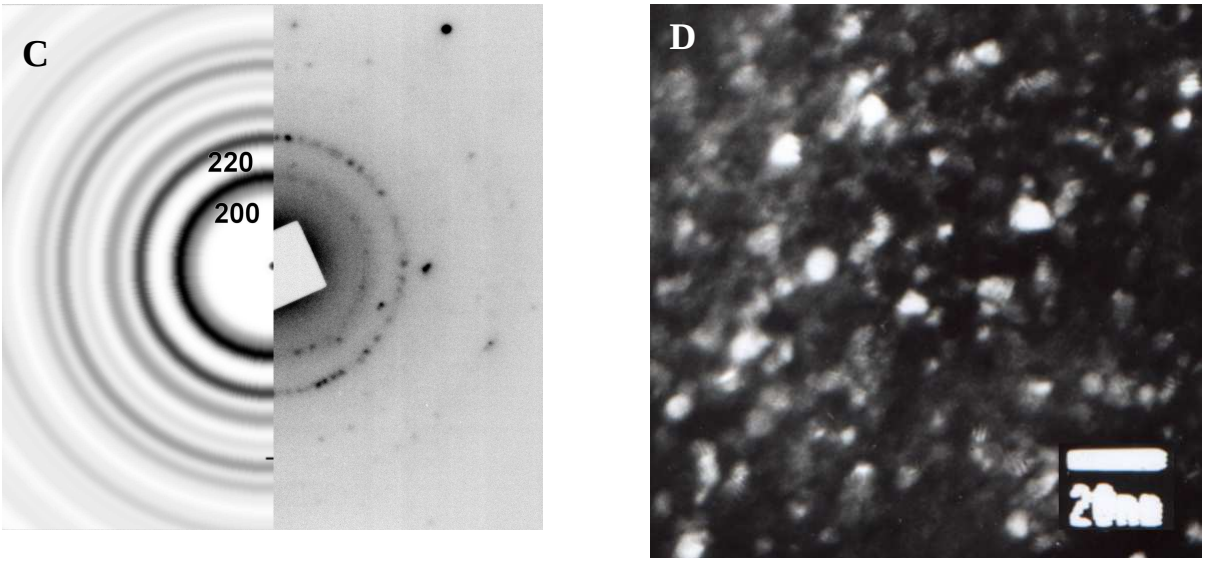

Figure (16) : TEM micrograph (cross section – A), and high-resolution TEM (HRTEM) image and a FFT (Fast Fourier Transform) of the image (inset) – B of a thin film, thermally treated at 230 ^{o}C for 15 min. In Figure C the right hand side represents the experimental diffraction pattern of the sample and the left hand side the simulated diffraction pattern for cubic NiO, while Fig. D shows the in plan-view of a thin film thermally treated at 300 ^{o}C for 15 min.

TEM micrographs of the optimised film deposited in SnO_2/F glass (Figure 16) shows a layer with a thickness of 35 ± 5 nm (A). The layer was not uniform as in the case of the $NiSO_4$ precursor. It adopted the morphology of the substrate itself, which was not smooth (Fig. 8A). In the groove at the grain boundary of two well-crystallized SnO_2 grains, the thickness of the film was approximately 45 nm. From the HRTEM (Fig. 16B) it is evident that the diameter of nano-grains (areas with darker contrast and rounded shape where lattice fringes could be seen) was up to 5 nm. They were embedded in an amorphous phase (brighter contrast). The inset in Fig. 16B presents the fast Fourier Transform (FFT) of the HRTEM image. The spots could be indexed as (111) and (200) planes of cubic NiO. From the FFT image we could conclude that the grains were crystallographically randomly oriented. The right hand side in Fig. 16C represents the experimental diffraction pattern, while the left side the simulated diffraction pattern for cubic NiO (bunsenite). A 2 nm particle size was taken for the calculated diffraction. The actual grains were larger (see Fig. 16B) but due to the poor crystallinity of the grains the best fit between the calculated and experimental patterns was obtained for smaller grains.

2. 3 Comparison of the results obtained for sol-gel prepared thin films from $NiSO_4$ and $Ni(CH_3COO)_2$ precursors :

2.3.1 TG and EXAFS measurements

The choice of precursor for sol-gel prepared Ni oxide thin films very much influences the properties of the final electrochromic material. The first difference between them is the temperature at which thermal decomposition of the sol-gel prepared thin film begins, leading to formation of Ni oxide phase. An approximately 50 degrees higher onset temperature was obtained for films prepared from $NiSO_4$ precursor (280 ^oC) than for films prepared from $Ni(CH_3COO)_2$ precursor (230 ^oC).

The EXAFS results (Figure 17) show that thermal treatment increased order in the vicinity of the Ni atoms. The films from $Ni(CH_3COO)_2$ precursor showed a higher degree of crystallization during heat-treatment than the thin films from $NiSO_4$ precursor, and this observation was in accordance with the TEM results. The first peak in the Fourier transforms was almost identical in all spectra, irrespective of the type of precursor and heat treatment applied. This agrees perfectly with the model with 6 equivalent oxygen neighbours. The observed Ni–O distance of 2.05 Å is characteristic of the NiO bunsenite structure. The second shell of neighbours reflects the ordering of the structure. Thermally untreated samples possessed a loose structure with a small portion of higher components. In thermally treated samples, the second-neighbour peak could be modelled by 12 Ni atoms at 2.98 Å as in bunsenite. The amplitude of the second peak in the film prepared from the sulphate precursor with completely decomposed acetate groups (Fig. 17A), was the same as of the film prepared from the acetate precursor (Fig. 17B), where thermal decomposition of acetates was 45 %. It seems that sulfate ions bonded to surface nickel atoms prevented nano grains from segregating.

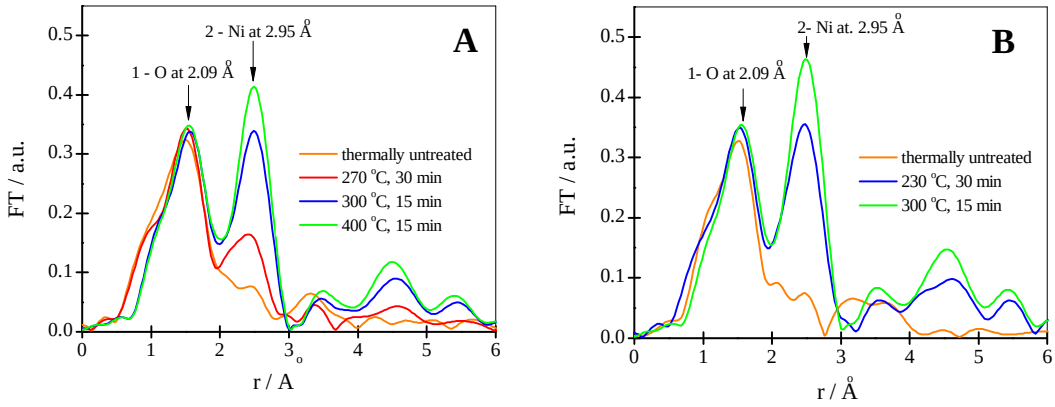

Figure (17) : Fourier transforms of k weighted EXAFS spectra of thin films, deposited on Al foil; k = 2.5 – 10.5 Å (A – $NiSO_4$ precursor; B – $Ni(CH_3COO)_2$ precursor). The first and the second neighbour peak were identified and the corresponding theoretical distances for bunsenite NiO are indicated.

2.3.2 Electrochromic properties of optimised films

In the case of the sulfate precursor, the film in which thermal decomposition of acetates was completed possessed an optimised electrochromic response. The calculated coloration efficiency after the activation period was – 41 $cm^2\ C^{-1}$ and the transmittance change between the bleached and the coloured state was 46.5 % at λ = 480 nm. In a 35 nm thick film, the size of the bunsenite nanograins reached 2 – 3 nm. Sulfate ions remained monodentately bonded to nickel, most probably in the surface of the grains.
In the optimised film prepared from nickel acetate precursor, thermal decomposition of acetates reached only 25 %, indicating that there was still a hogh proportion of amorphous phase in the structure. However, already at this stage the bunsenite grains grew much larger; their diameter was around 5 nm. In this film carbonate ions were present, originating from thermal decomposition of acetate groups. In the IR spectrum of this film the vibrations of carbonate ions were overwhelmed by the symmetric and asymmetric stretching vibration of acetates. In a more thermally treated film from the acetate precursor (60 min at 230 ^oC; 65 % decomposition of acetates), carbonate ions remained adsorbed in the structure or bidentately bonded to nickel. During the activation period the amorphous phase probably transformed into an electroactive phase. The electrochromic properties in the steady state (100^{th} cycle) were a little poorer as compared to the optimised film of $NiSO_4$ precursor, the coloration efficiency was – 38 $cm^2\ C^{-1}$ and the transmittance change 40.6 % at λ = 480 nm, which we attributed to the larger NiO grains.

Greater differences between optimized films from $NiSO_4$ precursor (60 min at 270 ^oC) and $Ni(CH_3COO)_2$ precursor (15 min at 230 ^oC) were observed at the beginning of cycling. The optical response of the film from the $Ni(CH_3COO)_2$ precursor was very small (11 %), whereas for the $NiSO_4$ precursor film it was 26 %. The electrochemical mechanism at the beginning of the cycling process was most likely different in the two films. *Ex-situ* infrared transmittance spectra (Fig. 18) of virgin and soaked films (prepared from $NiSO_4$ precursor) showed that sulfate ions were removed from the film after 5 min soaking in a solution of LiOH (Fig. 18, b). Instead of sulfate vibrations, bidentately bonded carbonate vibrations were observed, showing that in basic LiOH solution sulfate ions were replaced by hydroxide ions, which in air react with atmospheric CO_2 according to the reaction: $2OH^- + CO_2 \rightarrow CO_3^{2-} + H_2O$. The higher intensities of carbonate vibrations in the bleached state, characteristic of chelate bonding, favoured the reaction: $Ni(OH)_2$ (bleached) + $OH^- \leftrightarrows$ NiOOH (coloured) + $H_2O + e^-$ [69]. In the coloured state (Fig. 18, c) the strong and sharp band at 573 cm^{-1} corresponded to the Ni^{3+}–O stretching mode and that at 445 cm^{-1} to the NiO stretching vibration [1(a)]. The appearance of both vibrations indicated that in the coloured state both species, NiOOH and NiO existed simultaneously. This fact again confirmed that the colouration process occurred on the surface of the grains. The slight difference in frequencies observed the in spectra with respect to the reference ones [1(a)] was expected because of the different measurement mode. In the spectrum of the bleached film (Fig. 18, d) the band positioned at 573 cm^{-1} shifted to 591 cm^{-1}, corresponding to the Ni^{2+}–OH bending mode. The small peak at 3638 cm^{-1} corresponded to non-hydrogen bonds ν(OH), characteristic of the β(II)-$Ni(OH)_2$ phase. This means that already at the beginning of potential cycling the more compact layered structure of $Ni(OH)_2$ started to form.

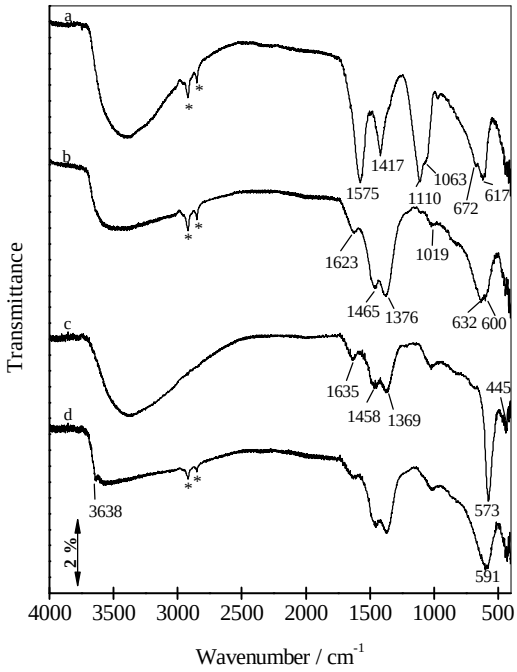

Figure (18) : *Ex-situ* IR transmittance spectra of a thin film prepared from the sulfate precursor and thermally treated at 270 °C for 15 minutes (a), after soaking for 5 minutes in 0.1 M LiOH (b), galvanostatically charged – coloured (c) and discharged – bleached (d). * denotes the absorbance of the glue deposited on the copper tape. The copper tape was stuck on the upper edge of the Si resin to enable better contact between Si and the external circuit.

For the acetate precursor a similar *ex-situ* measurement was not performed. Figure 19 respresents X-ray diffractograms of thermally untreated films of both precursors and of both optimized films in the range from 5 to 20 degrees 2 Θ. At higher angles no diffraction peaks were observed. The broad peak positioned at low angles is characteristic of the less ordered structure of the turbostratic layered structure of α(II)-$Ni(OH)_2$ [5, 26(b), 27(a)]. The calculated interplanar distance along the c-axis in both thermally untreated films (Fig. 19, a, c) is from 9.5 to 10.5 Å. A layer of water molecules is inserted between the $Ni(OH)_2$ slabs in the α-phase, resulting in a higher diffusion coefficient and consequently good intercalation properties (also fast kinetics) with regard to the β-phase. A high decrease in transmittance was observed in the beginning of the cycling in both thermally untreated films. But already in the 1st cycle the bleaching process was not reversible due to the instability of the α-phase in the alkaline electrolyte [70]. The α-phase totally disappeared in the XRD spectrum of the optimised film prepared from $NiSO_4$ precursor (Fig. 19, b). Thermal decomposition of acetate groups is complete, and the film was composed of NiO grains on the surface where the elecrochromic reaction took place. On the contrary, there is still much thermally undecomposed amorphous phase in the optimized film prepared from $Ni(CH_3COO)_2$ precursor. In the XRD spectrum a broad peak with lower intensitiy with regard to thermally untreated film was still observed in this range (Fig. 19, d), meaning that this film was composed of at-least two structures: NiO grains with an average size of 5 nm and turbostratic α-$Ni(OH)_2$ phase. Some carbonate ions, originating from thermal decomposition of acetate groups, were also

bonded in the structure. It was reported that planar carbonate ions are totally hydrogen bonded to water molecules in the interslab space, which increase the stability of this material [71]. Two possibilities of answering the question regarding the different mechanisms of the two optimized films at the beginning of cycling would therefore be: (i) the presence of carbonate ions in the thermally undecomposed layered structure in the film of $Ni(CH_3COO)_2$ precursor (more time is probably needed for them to be exchanged with hydroxide ions than for sulfate ions present in the film of $NiSO_4$ precursor), (ii) the size of the nano-grains which grew larger in the film prepared from the acetate precursor.

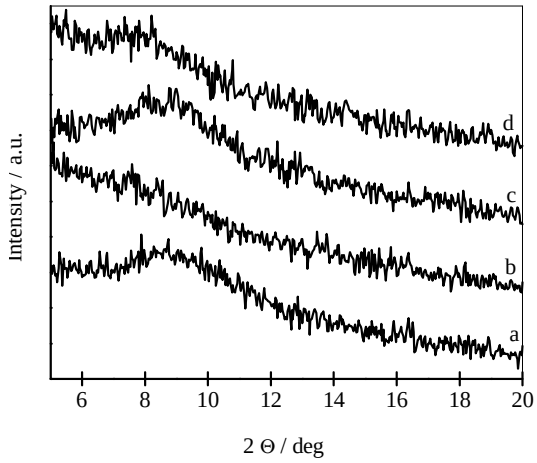

Figure (19) : X-ray diffractograms of thin films, deposited on Si resin. Thermally untreated film prepared from the sulfate precursor (a), and thermally treated for 60 min at 270 ^oC (b); thermally untreated film prepared from the acetate precuros (c), and thermally treated for 15 min at 230 ^oC (d).

2.4 Thin films prepared by alternately dipping deposition (ADD) from nickel sulfate precursor

2.4.1 Preparation of the sol and xerogel; thin film deposition :

Thin films were prepared on different substrates by the ADD technique. First, a wetting agent was dispersed on the substrate with a pulling velocity of 5 cm min^{-1}. The same wetting agents for different substrates (Pt foil, Si resins, SnO_2/F glass) were used as described in 2.1.1. After the wetting solution had dried, thin films were prepared by alternately immersing the substrates in two solutions, the first of 0.05 mol L^{-1} $NiSO_4$ (Kemika, Zagreb, Croatia) and the other of 0.05 mol L^{-1} LiOH (Kemika). Consequently a thin film of light green amorphous nickel hydroxide was formed on the substrate. The thickness of the thin film increased with the number of immersions, as confirmed by observation. For TG measurements, thin films were deposited on platinum foil. For FT-IR analysis silicon resins polished on both sides were used as substrates. The number of immersions was 7 for each solution. For *in-situ* spectroelectrochemical measurements, SnO_2/F glass was used as the substrate. The number of immersions was again 7. The xerogel used in TG and XRD

measurements was obtained by mixing equal volumes of 0.1 M $NiSO_4$ and 0.1 M LiOH, centrifuged, cast in a Petri dish and dried in air at ambient temperature.

2.4.2 Thermogravimetric measurements :

A comparison of dynamic TG measurements of a thin film deposited on a Pt foil, and the corresponding xerogel is presented in Figure 20. There was a great difference in the course of thermal decomposition of the thin film sample (dotted curve) with respect to that of the xerogel (solid curve). The first step in the weight loss curve could be ascribed to dehydration of adsorbed water and elimination of intercalated water, and this occurred for both samples up to 200 °C. Then the thermal decomposition of nickel hydroxide to nickel oxide began according to the reaction $Ni(OH)_2 \rightarrow NiO + H_2O$ [72], which is evident from the second step of the TG curve.

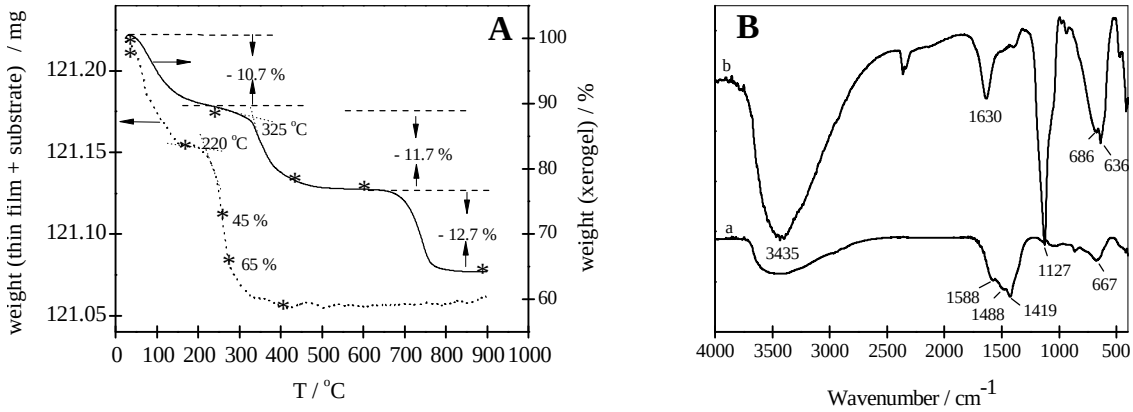

Figure (20) : Dynamic TG curves of a thin film (left ordinate) and of the powdered xerogel (right ordinate) in a dynamic air atmosphere – A. The initial weight of the thin film and substrate was 121.218 mg, while that of the powder was 9.880 mg. The IR spectra of the thermally untreated thin film, deposited on Si resin (a) and the xerogel (b), are presented in Figure B.

Thermal decomposition of the thin film started at a temperature 100 °C lower (220 °C) than that of the corresponding xerogel (325 °C). It is known that in dynamic measurements the decomposition temperature decreases with decrease in sample particle size [58] since decomposition products have first to diffuse to the surface of the solid particle before they evolve. This process takes longer in the case of larger particles, while the temperature in dynamic measurements is increasing. Therefore decomposition temperatures for xerogel samples with an average size of some μm are shifted towards higher values in comparison with thin films with a thickness of some tens of a nm. On the basis of our previous examination this temperature difference was around 30 °C [1(b,c)], so we concluded that there should be another reason in this case for such a large difference in the thermal stability of the precipitated $Ni(OH)_x$ thin film with respect to the xerogel, most probably due to the different counter-ion. Lithium and sulfate ions were present in the structure due to the mode of preparation of the samples. Comparison of the IR spectra (Fig. 20B) for the thin film and the xerogel showed that there was a high concentration of sulfate ions in the xerogel

sample, while in the thin film sample carbonate ions are predominant. Sufate ions in the xerogel were either intercalated in the structure (the peak positioned at 1127 cm^{-1} is characteristic of sulfate ions with T_d symmetry) or monodentately bonded to nickel cations, corresponding to bending modes of sufates at 686 and 636 cm^{-1} [68]. In the IR spectrum of the thin film the bands positioned at 1488, 1419 and 861 cm^{-1} revealed the presence of adsorbed carbonate ion with planar D_{3h} symmetry, while the band at 1588 cm^{-1} corresponded to bidentately coordinated carbonate ions [68]. The origin of the carbonate ions was from atmospheric CO_2 which was chemisorbed on the basic surface after the thin film had been withdrawn from the LiOH solution. Reichle [73] reported that in layered hydroxides the order of affinity towards anions is: $CO_3^{2-} > SO_4^{2-}$, $OH^- > F^- > Cl^-$. During the ADD process the excess of negative sulfate ions (caused by carbonate insertion) precipitated in the thin film must return into solution due to the electroneutrality condition. For the bulk material (xerogel) no evident insertion of carbonate ions took place. The reason is that the huge surface area of the amorphous $Ni(OH)_x$ precipitated on the substrate acts as a nanostructured material. Many of the atoms are on the surface, allowing a nearly stoichiometric surface – gas reaction [74]. Carbonates are less thermally stable than sulfates. The mixture of $NiCO_3$ and $Ni(OH)_2$ thermally decomposed at 400 °C, while thermal decomposition of $NiSO_4$ was complete only at 900 °C [75]. Sulfate ions in the xerogel therefore stabilized the $Ni(OH)_2$ structure and decomposition began at a higher temperature. The third step in the TG curve of the xerogel above 600 °C was a result of the decomposition of $NiSO_4$ to NiO [6].

Figures 21 A and B present the isothermal TG curve at 220 ^oC of a thin film deposited on a Pt foil. In Fig. 21A the temperature profile in the furnace is presented on the right- hand axis and on the left-hand axis the weight of the film on the substrate on a percentage scale. The first step in the TG curve occurred during linear heating and was due to dehydration. Thermal decomposition of nickel hydroxide to oxide occurred after the furnace reached its isothermal temperature and was fast in the beginning, but became slow with increasing time. After 120 min the decomposition of anhydrous hydroxide to oxide reached 60 %, as marked in Fig. 21B, which presents the temperature dependence of the same data. The temperature in the furnace was increased again after 180 min at 220 ^oC to a final temperature of 400 ^oC, where decomposition to nickel oxide was complete (100 %).

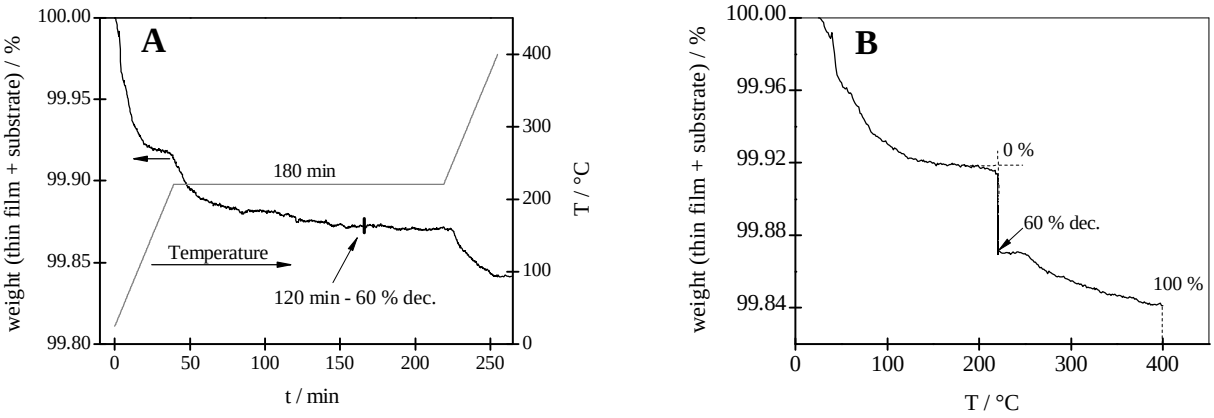

Figure (21) : Isothermal TG curves of a thin film deposited on a platinum foil at 220 °C; time dependence – A and temperature dependence – B.

2.4.3 *In-situ* spectroelectrochemical measurements :

In-situ monochromatic optical transmittance changes (λ = 480 nm) during chronocoulometric measurements of thin films thermally treated to different degrees are shown in Figure 22. Fig. 22A represents the response at the beginning of the cycling experiment, while 22B shows the stabilised 101st cycle during charging at a potential of 0.6 V vs. Ag/AgCl (0 – 30 s) and discharging at 0.0 V vs. Ag/AgCl (30 – 60 s). At the beginning of cycling, the highest degree of coloration was shown by a thin film where the degree of thermal decomposition from amorphous anhydrous nickel hydroxide to oxide was 25 % (120 min at 215 ^{o}C). After prolonged cycling, the decrease of transmittance in the bleached state of 15 % indicated that the colouring / bleaching process was not reversible. The change in transmittance during the 2nd coloration was only 15 % for a thin film exposed for 120 min at 220 ^{o}C (60 % decomposition), but in the 101st cycle it reached a better value (43 %) than the film with 25 % decomposition (27 %). After the 101st bleaching process, the decrease in transmittance showed that reversibility was not yet achieved (Fig. 22B). An optimal optical response in the 101st cycle was exhibited by a film with 65 % decomposition (120 min at 235 ^{o}C); the calculated coloration efficiency reached – 37 cm^{2} C^{-1}, while at the beginning of cycling the CE was – 32 cm^{2} C^{-1}. For more thermally treated films the optical modulation was lower with respect to the optimized film. From Fig. 22B we can see that it took around 5 s to colour films with 25 % decomposition and 90 % decomposition, while films with 60 and 65 % decomposition needed more time (approx. 15 s). It is interesting that a longer time was needed for films with better performances, while less time was needed for those thermally treated to an insufficient degree (too less or too much). This behaviour was also observed in the case of sol-gel prepared films.

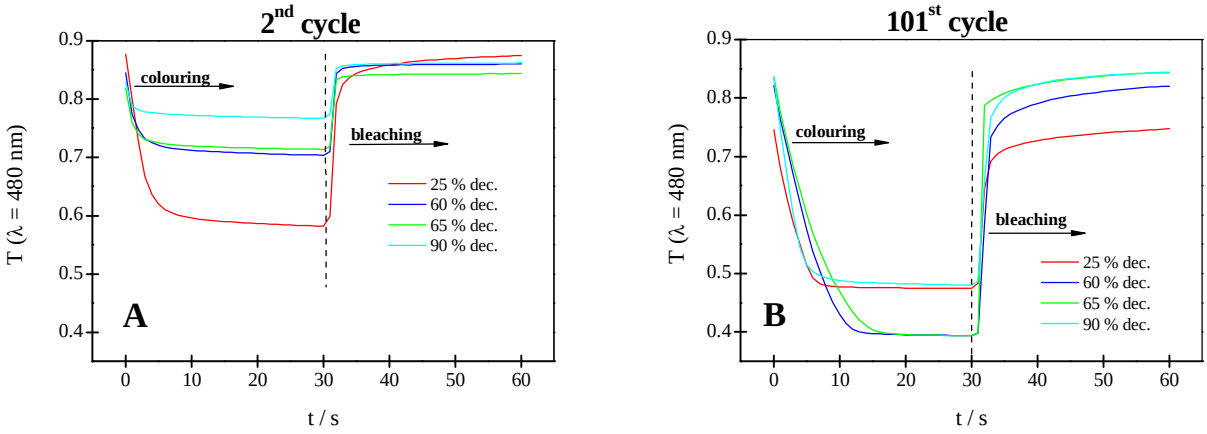

Figure (22) : *In situ* monochromatic optical transmittance changes (λ = 480 nm) during chronocoulometric measurements of thin films thermally treated to different degrees (2nd cycle – A, 101st cycle – B). The films were coloured at 0.6 V for 30 s and bleached at 0.0 V for 30 s.

The evolution of the cyclovoltammetric curves and the corresponding *in-situ* monochromatic transmittance changes of the optimized film (65 % decomposition – 120 min at 235 °C) are shown in Figures 23A and B. This film exhibited excellent reversibility in the 101st cycle. At the beginning of cycling the basic form of the

cyclovoltammetric curve was not yet developed (Fig. 23A). During the cycling process current densities became larger. The anodic and cathodic peaks became more and more pronounced, and the potential difference between them larger, indicating loosening of the structure. The changes in transmittance between the bleached and coloured state increased from 13 % in the 1st cycle to 45 % in the100th cycle.

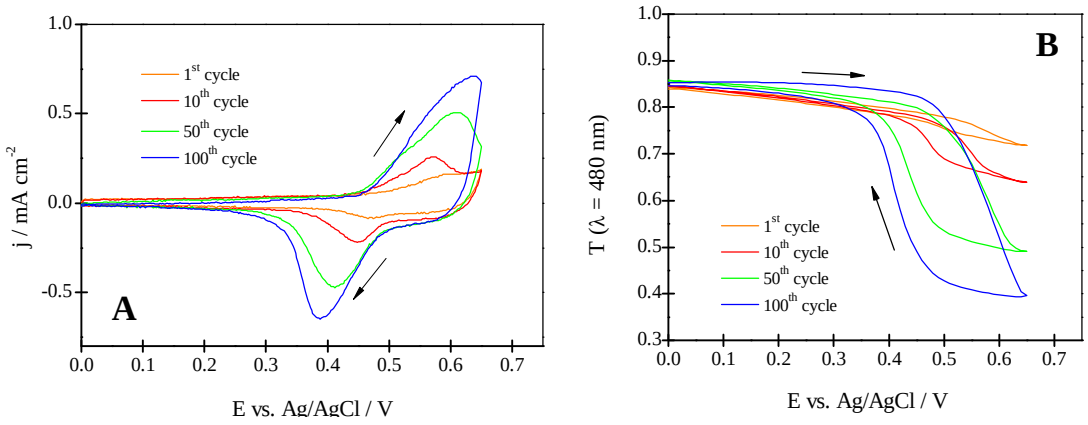

Figure (23) : Cyclovoltametric curves – A, and monochromatic transmittance changes – B of the optimized film (65 % decomposition – 120 min at 235 °C).

2.4.4 Structural and morphological measurements :

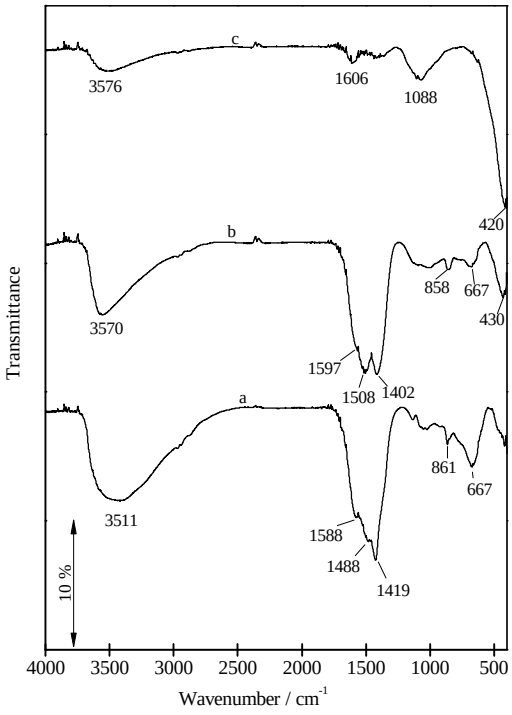

Figure (24) : IR transmittance spectra of thin films thermally treated to different degrees: thermally untreated film (a), 65 % decomposition (b) and 100 % decomposition (c).

IR spectra of thin films deposited on silicon resin and thermally treated to different extents are shown in Figure 24. The IR spectrum of the thermally untreated thin film is described in the paragraph where the difference in thermal stability between a thin film and the xerogel is explained. It the film where thermal decomposition of anhydrous hydroxide reached 65 % (b), the band at 667 cm^{-1} arose from the bending vibration of δ(Ni–OH). After dehydration the shape of the spectrum resembled the spectrum of layered turbostratic $Ni(OH)_2$ [26(b)], on which vibrations of carbonate ions were superimposed. With a higher degree of thermal decomposition, the band for stretching Ni–O vibrations became more and more intense. The intensities of bands for carbonate ions diminished during heat treatment. Besides the intense Ni–O stretching vibration, there were two peaks due to adsorbed moisture and a peak of the silicon substrate (1088 cm^{-1}) in the spectrum of the film thermally treated up to 400 ^{o}C.

TEM micrographs of the optimized thin film (thermal treatment for 120 min at 235 ^{o}C; 65 % decomposition of anhydrous hydroxide) are presented in Figures 25A, B. The microstructure of the optimized film was not as well developed as in the case of the films prepared by the sol-gel method [1(d)]. It consisted of particles (flakes) with a size from 20 to 50 nm, and there was also some inner porosity. The open porosity of this sample enabled diffusion of LiOH during the cycling process through the whole thickness of the layer. From the FT-IR spectrum it is evident that the film consisted of two structures: nickel hydroxide with inserted and bidentately coordinated carbonate ions and nickel oxide. The thickness of the film was around 300 nm (Fig. 25A). The high resolution TEM (HRTEM) image and the Selected Area Electron Diffraction (SAED) pattern (Fig. 25B with inset) of a cross section of the thin film showed that the film was composed of an amorphous phase and a few nanometre (2-3 nm) sized crystalline particles. In the SAED pattern, where the well defined diffraction spots originate from the silicon substrate, the faint and diffuse circle corresponded to the (002) plane of cubic NiO (marked with an arrow). Between the silicon monocrystalline substrate and the NiO nanoparticles there was a continuous amorphous layer around 2 nm thick, indicating that NiO particles were formed during heat treatment by homogeneous nucleation.

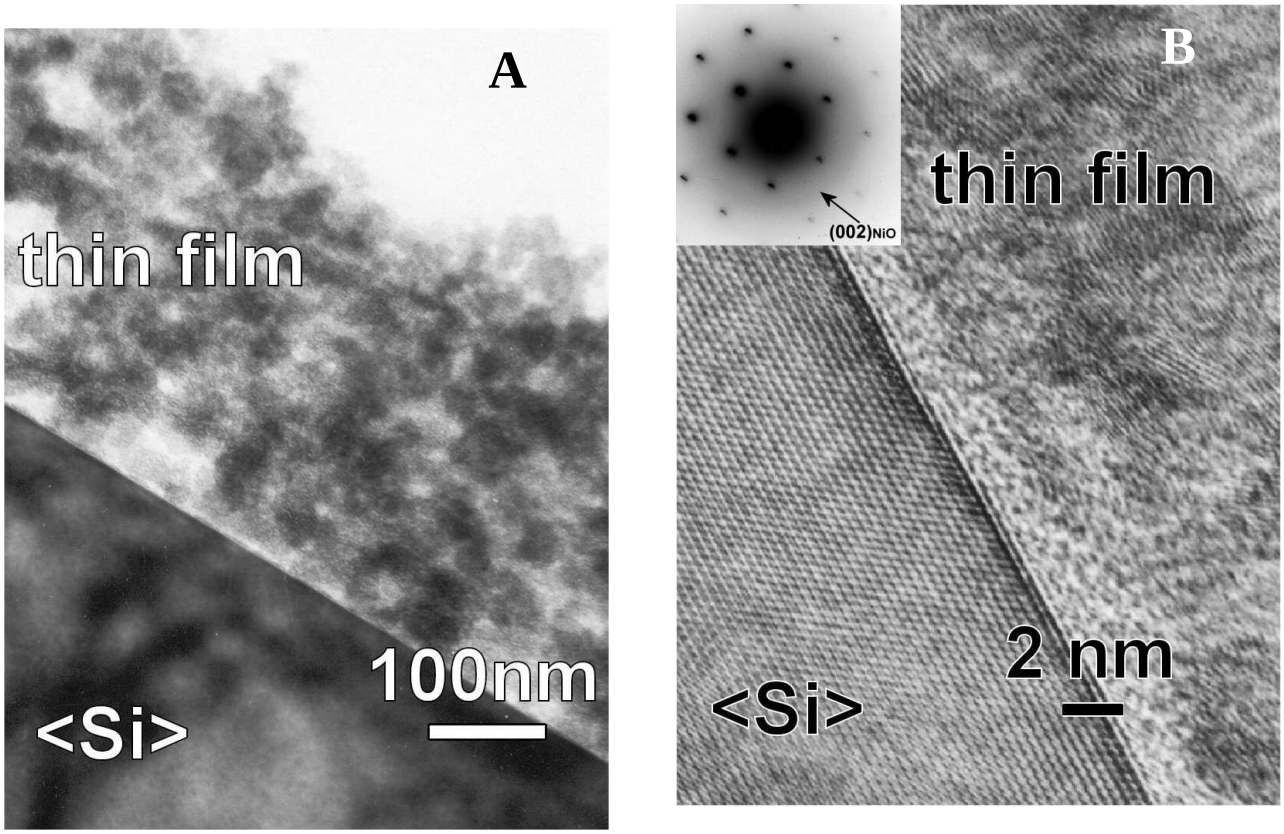

Figure (25) : TEM micrographs of the optimised film prepared by the ADD technique.

2.4.5 Final remarks :

Comparison of dynamic TG measurements made on ADD prepared thin films and the corresponding xerogels suggested that the two samples differ in more than sample size. The observed difference in onset decomposition temperature of nickel hydroxide was more than 100 ^{o}C. For sol-gel prepared samples the difference in the onset decomposition temperature was around 30 ^{o}C [1(b,c)]. Besides, the xerogel sample exhibited a third step in the dynamic TG curve in the range from 600 to 800 ^{o}C, while the TG curve of the thin film was flat in this range. With the help of FT-IR spectroscopy it was found that sulfate ions were replaced by carbonate ions in thin film samples, most probably during the ADD process when the sample was repeatedly pulled out of the solution. In this process, atmospheric CO_2 reacted with hydroxide ions leading to carbonate formation. We conclude that all sulfate ions were exchanged for carbonate ones since in the FT-IR spectrum there is no evidence of sulfate vibrations. Sulfate ions returned to solution but we did not investigate the mechanism of this process. For the xerogel sample, which we prepared by mixing equal volumes of the two solutions, this process could not happen.
The film where decomposition of nickel hydroxide was 65 % possessed an optimised electochromic response up to 101st cycle. From the FT-IR spectrum it was evident that it was composed of two structures: layered nickel hydroxide with inserted and bidentately coordinated carbonate ions, and nickel oxide. The TEM micrograph showed a thin film with a thickness of 300 nm which consisted of flakes 20 – 50 nm in size. Inside the flakes NiO nanoparticles (2-3 nm in diameter) were embedded in an amorphous matrix (Figs. 25A, B). Optical modulation of less thermally treated films

was better at the beginning of cycling, but poorer in the 101st cycle with regard to the optimized film. The bleaching process was not reversible, and the coloration less intensive than for the optimized film. Optical modulation of more thermally treated films (> 65 %) was lower with regard to the optimized film (Fig. 22B). Results obtained from sol-gel prepared films showed that thermal decomposition occurred at lower temperature in the samples which contained carbonate ions as compared to samples which contained sulfate ions. Carbonates probably hold the amorphous structure tightly together. Consequently they are scarcely exchanged with OH^- to obtain an electrochromically active $Ni(OH)_2$ phase, leading to poorer response at the beginning of cycling. TEM showed that the performance of films which consisted of only NiO phase (100 % decomposition) depended on the grain size and crystallinity. In the case when the size of the nanograins reached 5 nm in diameter, the film became electrochemically active during cycling [6]. After 14 hours the change in transmittance between the coloured and bleached state reached 30 % [43]. A film of 10 nm NiO grain size remained electrochemically inert, probably due to its lower active surface size on one hand, and to the increase in crystallinity on the other.

3. Conclusions :

The degree of the thermal treatment required to obtain electrochromic nickel-oxide thin films with maximal EC response depended strongly on the precursor used and on the chosen chemical route for their preparation. There is no explicit rule for the extent of treatment needed to obtain optimum properties. Counter-ions (sulfates, acetates etc.) play an active role in the formation of the structure and in the mechanism of the coloration.

Once optimal thermal treatment has been established for a certain system, it can be routinely used for further purposes. A future prospect is therefore the preparation of other types of thin films using different nickel salts or different wet preparation methods and optimization of their electrochromic response.

In searching for the optimal thermal treatment, the procedure is similar to numerical calculation of the zero value of a polynomial function. The approach from one side is to achieve reversible bleaching for films thermally treated to an insufficient degree (which means more thermal treatment, i.e. a higher temperature and/or longer duration) and from the other, a greater change in transmittance for films thermally treated at too high temperature (less thermal treatment; i.e. lower temperature and/or shorter duration). For this method of optimization we need two sets of information - isothemal thermogravimertic (TG) measurements of thin films at a certain chosen temperature, and cyclovoltammogramms (CV) or chronopotentiometric measurements (CPC) for a number of cycles for films already thermally treated to a certain degree at this temperature.

Due to differences in sample size and sometimes the different chemical composition of thin films and the corresponding xerogels, thermogravimertic measurements should be made on thin films deposited on the substrate under conditions equal to those for thermal treatment of large-area samples.

4. References :

[1] (a) A. Šurca, B. Orel, R. Cerc-Korošec, P. Bukovec, and B. Pihlar, J. Electroanal. Chem. 433 (1997) 57. (b) R. Cerc Korošec, P. Bukovec, B. Pihlar, and J. Padežnik Gomilšek, Thermochim. Acta 402 (2003) 57. (c) R. Cerc Korošec, and P. Bukovec; Thermichim. Acta 410 (2004) 65. (d) R. Cerc Korošec, P. Bukovec, B. Pihlar, A. Šurca Vuk, B. Orel, and G. Dražić, Solid State Ion. 165 (2003) 191.

[2] P. S. Patil, S. B. Nikam, and L. D. Kadam, Mater. Chem. Phys. 69 (2001) 77.

[3] (a) T. Maruyama, and S. Arai, Sol. Energ. Mater. Soll. Cells 30 (1993) 47. (b) J. R. V. Garcia, E. M. L. Ugalde, F. H. Santiago, J. M. H. Lopez, J. Nanosci. Nanotechnol. 8 (2008) 2703.

[4] B. Pejova, T. Kocareva, M. Najdoski, and I. Grozdanov, Appl. Surf. Sci. 165 (2000) 271.

[5] M. A. Vidales-Hurtado, and A. Nendoza-Galván, Mater. Chem. Phys. 107 (2008) 33.

[6] R. Cerc Korošec, J. Šauta Ogorevc, P. Draškovič, G. Dražić, and P. Bukovec, Thin Solid Films 516 (2008) 8264.

[7] I. Porqueras, and E. Bertran, Thin Solid Films 398-399 (2001) 41.

[8] C. Natarajan, S. Ohkubo, and G. Nogami, Solid State Ion. 86-88 (1996) 949.

[9] K.-W. Nam, and K.-B. Kim, J. Electrochem. Soc. 149 (2002) A346.

[10] A. Agrawal, H. R. Habibi, R. K. Agrawal, J. P. Cronin, D. M. Roberts, R. S. Caron-Popowich, and C. M. Lampert, Thin Solid Films 221 (1992) 239.

[11] S.-H. Lin, F.-R. Chen, and J.-J. Kai, Appl. Surf. Sci. 254 (2008) 3357.

[12] F. F. Ferreira, M. H. Tabaanics, M. C. A. Fantini, I. C. Faria, and A. Gorenstein, Solid State Ion. 86-88 (1996) 971.

[13] B. Subramanian, M. M. Ibrahim, V. Senthilkumar, K. R. Murali, VS. Vidhya, C. Sanjeeviraja, and M. Jayachandran, Phys. B 403 (2008) 4104.

[14] C. G. Granqvist, Handbook of Inorganic Electrochromic Materials. (Elsevier, New York, 1995, reprinted 2002).

[15] A. Azens, and C. G. Granqvist, J. Solid State Electrochem. 7 (2003) 64.

[16] (a) S. A. Mahmoud, A. A. Akl, H., Kamal, and K. Abdel-Hady, Phys. B 311 (2002) 366. (b) A. J. Varkey, and A. F. Fort, Thin Solid Films 235 (1993) 47. (c) G. Boschloo, and A. Hagfeldt, J. Phys. Chem. B 105 (2001) 3039.

[17] (a) G. Eranna, B. C. Joshi, D. R. Runthala, and R. P. Gupta, Crit. Rev. Solid State Mater. Sci. 29 (2004) 111. (b) I. Hotovy, V. Rehacek, P. Siciliano, S. Capone, and L. Spiess, Thin Solid Films 418 (2002) 9. (c) I. Hotovy, J. Huran, P. Siciliano, S. Capone, L. Spiess, and V. Rehacek, Sens. Actuators B 78 (2001) 126. (d) J. A. Dirksen, K. Duval, and T. A. Ring, Sens. Actuators B 80 (2001) 106.

[18] V. Biju, Mater. Lett. 62 (2008) 2904.

[19] H. Sato, T. Minami, S. Takata, and T. Jamada, Thin Solid Films 235 (1993) 27.

[20] (a) G. A. Niklasson, and C. G. Granqvist, J. Mater. Chem. 17 (2007) 127. (b) C. G. Granqvist, E. Avendaño, and A. Azens, Thin Solid Films 442 (2003) 201. (c) C. G. Granqvist, G. A. Niklasson, and A. Azens, Appl. Phys. A – Mater. Sci. Process. 89 (2007) 29. (d) C. G. Granqvist, S. Green, E. K. Jonson, R. Marshal, G. A. Niklasson, A. Roos, Z. Topalian, A. Azens, P. Georén, G. Gustavsson, R. Karmhag, J. Smulko, and L. B. Kish, Thin Solid Films 516 (2008) 5921. (d) R. Cerc Korošec, and P. Bukovec, Acta Chim. Slov 53 (2006) 136.

[21] A. Nattestad, M. Ferguson, R. Kerr, Y. B. Cheng, and U. Bach, Nanotechnology, 19 (2008) 295304. (b) H. Zhu, A. Hagfeldt, and G. Boschloo, J. Phys. Chem. 111 (2007) 17455.
[22] Y. Zhou, D. H. Gu, Y. Y. Gen, and F. X. Gan, Mater. Sci. Eng. B: Solid-State Mater. Adv. Technol. 135 (2006) 125.
[23] U. M. Patil, R. R. Salunkhe, K. V. Gurav, and C. D. Lokhande, Appl. Surf. Sci. 255 (2008) 2603.
[24] (a) A. Pennisi, F. Simone, G. Barletta, G. Di Marco, and M. Lanza, Electrochim. Acta 44 (1999) 3237. (b) C. M. Lampert, Proc. SPIE 4458 (2001) 95. (c) M. L. Persson, and A. Roos, Energy Build. (to be published).
[25] G. Sarawadekar, and J. P. Agrawal, Def. Sci. J. 58 (2008) 486.
[26] (a) H. Bode, K. Dehmelt, and J. Witte, Electrochim. Acta 11(1966) 1079. (b) P. Oliva, J. Leonardi, J. F. Laurent, C. Delmas, J. J. Braconnier, M. Figlarz, and F. Filvet, J. Power Sources, 8 (1982) 229.
[27] (a) C. Faure, C. Delmas, and M. Fouassier, J. Power Sources 35 (1991) 279. (b) C. Faure, C. Delmas, and P. Willmann, J. Power Sources 35 (1991) 263.
[28] (a) P. C. Yu, G. Nazri, and C. M. Lampert, Sol. Energ. Mater. 16 (1987) 1. (b) K. Yoshimura, T. Miki, S. Tanemura, Jpn. J. Appl. Phys. 34 (1995) 2440. (c) A. Šurca, B. Orel, B. Pihlar, and P. Bukovec, J. Electroanal. Chem. 408 (1996) 83. (d) A. Nemetz, A. Temmink, K. Bange, S. I. Cordoba-Torresi, C. Gabrielli, R. Torresi, and A. Hugot-Le Goff, Sol. Energ. Mater. Soll. Cells 25 (1992) 93. (e) M. A. Vidales-Hurtlado, And A. Mendoza- Galván, Solid State Ion. 179 (2008) 2065.
[29] S. I. Cordoba-Toressi, A. Hugot-Le Goff, and S. Joiret, J. Electrochem. Soc. 138 (1991) 1554.
[30] S. I. Cordoba-Torresi, C. Gabrielli, A. Hugot-Le Goff, and R. Torresi, J. Electrochem. Soc., 138 (1991) 1548.
[31] I. Bouessay, A. Rougier, and J.-M. Tarascon, J. Electrochem. Soc. 144 (2004) H145.
[32] (a) E. Avendaño, L. Berggren, G. A. Niklasson, C. G. Granqvist, and A. Azens, Thin Solid Films 496 (2006), 30. (b) E. L. Miller, and R. E. Rocheleau, J. Electrochem. Soc. 144 (1997) 1995.
[33] (a) X. Chen, X. Hu, and J. Feng, Nanostruct. Mater. 6 (1995) 309. (b) Z. Xuping, and C. Guoping, Thin Solid Films 298 (1997) 53.
[34] W. Estrada, A. M. Andersson, and C. G. Granqvist, J. Appl. Phys. 64 (1988) 3678.
[35] I. Bouessay, A. Rougier, P. Poizot, J. Moscovici, A. Michalowicz, J.-M. Tarascon, Electrochim. Acta 50 (2005) 3737.
[36] (a) T. Miki, K. Yoshimura, Y. Tai, M. Tazawa, P. Jin, and S. Tanemura, The 3rd IUMRS International Conference on Advanced Materials, Tokyo, Japan, August 31 – September 4, 1993 KP12. (b) K. K. Purushothaman, and G. Muralidharan, J. Sol-Gel Sci. Technol. 46 (2008) 190.
[37] (a) C. J. Brinker, and G. W. Scherer, Sol-gel Science, The Physics and Chemistry of Sol-Gel Processing. (Academic Press, Boston, 1990). (b) L. L. Hench, and J. K. West, Chem. Rev. 90 (1990) 33. (c) M. Kikihana, J. Sol-Gel Sci. Techol. 6 (1996) 7.
[38] (a) P. K. Sharma, M. C. A. Fantini, and A. Gorenstein, Solid State Ion. 113-115 (1998) 457. (b) L. Županc-Mežnar, B. Praček, B. Orel, P. Bukovec, Thin Solid Films 317 (1998) 336.
[39] G. J. Exarhos, and X. D. Zhou, Thin Solid Films 515 (2007) 7025.

[40] (a) A. F. Wells, Structural Inorganic Chemistry, 4th Edition (Clarendon Press, Oxford, 1975, p. 445). (b) E. Antolini, J. Mater. Sci. 27 (1992) 3335. (c) Y. M. Lu, W. S: Hwang, and J. S. Yang, Surf. Coat. Technol. 155 (2002) 231.
[41] D. Adler, and J. Feinleib, Phys. Rev. B 2 (1970) 3112.
[42] X. H. Xia, J. P. Tu, J. Zhang, X. L. Wang, W. K. Zhang, and H. Huang, Electrochim. Acta 53 (2998) 5721.
[43] M. C. A. Fantini, G. H. Bezerra, C. R. Carvalho, and A. Gorenstein, Proc. SPIE 1536 (1991) 81.
[44] (a) S.-H. Lin, F.-R. Chen, and J.-J. Kai, Appl. Surf. Sci. 254 (2008) 3357. (b) M.-S. Wu, and C.-H. Yang, Appl. Phys. Lett. 91 (2007) 033109.
[45] K. Bange, and T. Gambke, Adv. Mater. 2 (1990) 10.
[46] A. Šurca, B. Orel, and B. Pihlar, J. Solid State Electrochem. 2 (1998) 38.
[47] A. M. Andersson, W. Estrada, C. G. Granqvist, A. Gorenstein, and F. Decker, Proc. SPIE 1272 (1990) 96.
[48] (a) M. Chigane, and M. Ishikawa, J. Electrochem. Soc. 141 (1994) 3439. (b) R. M. Torresi, M. V. Vázquez, A. Gorenstein, and S. I. Córdoba-Torresi, Thin Solid Films 229 (1993) 180.
[49] (a) A. Gorenstein, F. Decker, M. Fantini, and W. Estrada, Proc. SPIE 4 (1988) 272. (b) C. Natarajan, H. Matsumoto, and G. Nogami, J. Electrochem. Soc. 114 (1997) 121.
[50] K. J. Patel, C. J. Panchal, V. A. Kheraj, and M. S. Desai, Mater. Chem. Phys. 114 (2009) 475. (b) E. Ozkan, S. H. Lee, C. E. Tracy , J. R. Pitts, and S. K. Deb, Sol. Energy Mater. Sol. Cells, 79 (2003) 439. (c) A.A. Akl, H. Kamal, and K. Abdel-Hady, Phys. B. – Condens. Matter 325 (2003) 65. (d) Y. Shigesato, Jpn. J. Appl. Phys. 30 (1991) 1457.
[51] E. Hemmninger, and S. M. Sarge, in Handbook of Thermal Anaysis and Calorimetry, Principles and Practice; Edited by P. K. Gallagher, and M. E. Brown (Elsevier, Amsterdam, 1998), Vol.1, pp. 8-20.
[52] L. Niinistö, J. Therm. Anal. Cal. 56 (1999) 7.
[53] A. Šurca, B. Orel, B. Pihlar, J. Solid State Electrochem. 2 (1998) 389.
[54] Y. Sawada, and N. Mizutani, Netsu Sokutei 16 (1989) 185.
[55] M. Leskelä, P. Eskelinen, and M. Ritala, Thermochim. Acta 214 (1993) 19.
[56] P. K. Gallagher, W. R. Sinclair, R. A. Fastnacht, and J. P. Luongo, Thermochim. Acta 8 (1974) 141.
[57] (a) N. Tohge, A. Matsuda, and T. Minami, J. Am. Ceram. Soc. 70 (1987) C13. (b) M. Kumeda, H. Komatsu, and T. Shimizu, Thin Solid Films 129 (1985) 227. (c) J. R. Bosnell, and J. A. Savage, J. Mater, Sci. 7 (1972) 1235. (d) D.S. Easton, E. H. Henninger, O. B. Cavin, and C. C. Koch, J. Mater. Sci. 18 (1983) 2126.
[58] W. W. Wendlandt, Thermal methods of Analysis. (Interscience Publishers, New York, 1964, p. 17).
[59] M. Kawarada, and Y. Nishina, Japan. J. Appl. Phys. 16 (1977) 1531.
[60] R. Cerc Korošec, and P. Bukovec, J.Therm. Anal. Cal. 56 (1999) 587.
[61] M. Leskelä, T. Leskelä, and L. Niinistö, J. Thermal. Anal. Cal. 40 (1993) 1077.
[62] P. K. Gallagher, J. Thermal. Anal. 38 (1992) 17.
[63] (a) S. Lieb, R. K. MacCrone, J. Theimer, and E. W. Maby, J. Mater. Res. 1 (1986) 792. (b) J. Przyłuski, J. Płocharski, and W. Bujwan, J. Thermal. Anal. 21 (1981) 235. (c) S. Hackwood, G. Beni, and P. K. Gallagher, Solid State Ion. 2 (1981) 297.
[64] P. S. Gill, S. R. Sauerbrunn, and B. S. Crowe, J. Thermal. Anal. 38 (1992) 255.
[65] F. Nava, G. Ottaviani, and G. Riontino, Mater. Lett. 3 (1985) 3113.

[66] V. Balek, J. Fusek, O. Kriz, M. Leskelä, L. Niinistö, E. Nykänen, J. Rautanen, and P. Soininen, J. Mater. Res. 9 (1994) 119.
[67] Tuula Leskelä, Thermoanalytical Techniques in the Study of Inorganic Materials. (Dissertation, Helsinki University of Technology, Helsinki, 1996).
[68] K. Nakamoto: Infrared and Raman spectra of Inorganic and Coordination Copounds, 5th Edition (John Wiley & Sons, New York, 1997).
[69] (a) J. S. E. M. Svensson, and C. G. Granqvist, Solar Energy Mater. 16 (1987) 19. (b) G. Feuillade, and R. Jacoud, Electrochim. Acta 14 (1969) 1297.
[70] S. Le Bihan, J. Guenot, and M. Figlarz, C. R. Acad. Sci. 270 (1970) 2131.
[71] C. Faure, Y. Borthomieu, C. Delmas, and M. Fouassier, J. Power Sources 36 (1991) 113.
[72] (a) T. S. Horányi, Thermochim. Acta 137 (1989) 247. (b) Q. Song, Z. Tang, H. Guo, and S. L. I. Chan, J. Power Sources 112 (2002) 428.
[73] W. T. Reichle, Solid State Ion. 22 (1986) 135.
[74] K. J. Klabunde and R. S. Mulukutla, in: Chemical and Catalytic Aspects of Nanocrystals, Nanoscale Materials in Chemistry, Edited by K. J. Klabunde (Wiley, New York, 2001, p. 223).
[75] Atlas of Thermoanalytical Curves, Edited by G. Liptay. (Akadémiai Kiadó Budapest, 1977).